UNIVERSITÀ DEGLI STUDI DI PADOVA

FACULTY OF ENGINEERING

DEPARTMENT OF INDUSTRIAL ENGINEERING

THESIS IN ENERGY ENGINEERING

SEMI-EMPIRICAL MODELLING OF A MULTI-DIAPHRAGM PUMP INTEGRATED INTO AN ORC EXPERIMENTAL UNIT

Supervisors: Prof. Andrea Lazzaretto
Prof. Sotirios Karellas

Majoring: Filippo D'Amico

ACCADEMIC YEAR 2015 – 2016

Abstract

The study of the pump in an Organic Rankine Cycle (ORC) permits to find inefficiencies in a system that has in itself a low global efficiency. A key aspect of this study is the prevention of the cavitation that produces strong inefficiency and instability of the whole ORC system. The semi-empirical model proposed, after an accurate calibration of the pump system in the ORC unit taken into account, is able to predict the behaviour of the pump in different operating conditions, then it is possible to obtain its characteristic curves. For the cavitation problem the model is able to match its results with the experimental ones and find two-phase fluid at the same operating conditions. Thanks to this characteristic feature of the model it is possible to predict and avoid the cavitation during the operation of the experimental unit.
This thesis has been made in the Steam Boilers and Thermal Plants laboratory of the National Technical University of Athens during the Erasmus program period.

Sommario

Lo studio della pompa presente nel ciclo Rankine organico (ORC) permette di trovare inefficienze in un sistema che ha già di suo una bassa efficienza globale. Un aspetto chiave di questo studio è la prevenzione alla cavitazione che produce forti inefficienze ed instabilità dell'intero sistema ORC. Il modello semi empirico proposto, dopo un'accurata calibrazione del sistema pompa dell'unità ORC presa in considerazione, è in grado di prevedere il comportamento della pompa in differenti condizioni operative, quindi è possibile ottenere le sue curve caratteristiche. Per il problema della cavitazione il modello è in grado di ottenere risultati molto vicini a quelli sperimentali e trovare condizioni di fluido bifase nelle stesse condizioni operative. Grazie a questa caratteristica del modello è possibile prevedere ed eliminare la cavitazione durante il funzionamento dell'unità sperimentale.
Il lavoro di tesi è stato fatto nel laboratorio dell'Università Tecnica Nazionale di Atene durante il periodo del programma Erasmus.

Index

Introduction

One of the goal in energy field is the reduction of the pollutant emissions. To achieve this goal it is necessary the usage of the renewable sources, the recovery of waste heat and the maximization of the efficiency of the energy conversion processes.
The ORC plants are useful to exploit the waste heat and the heat from renewable sources, like geothermal and direct solar energy. There are different configurations of ORC plants: subcritical and supercritical, with many types of working fluids, usually hydrocarbons or CFCs, in function of the temperature of the source, cost, maximization of the power or any other constrains.
Researches have been done about nominal steady-state optimization, screening working fluid and operating conditions, and recently about off-design dynamic behaviours. [9,10,11,12]
Also the components have been optimized, the most critical is the expander and the are a lot of research about it [1,2,4,7,8], the heat exchangers and the evaporators are also investigated, but few researches have been done studying the pump [3,6,7]. However, Quoilin *et al.* (2013) describes the pump as a key component that should be carefully chosen according to its controllability, tightness, Net Positive Suction Head (NPSH) and efficiency. Pump efficiency becomes a crucial parameter for low temperature and supercritical cycles. Back Work Ratio defines as the ratio between pump electrical consumption and expander outlet power is introduced to evaluate pump impact, in the first chapter it is described how this parameter is worst for organic fluids compared to the water. Under these motivations and the necessity of the National Technical University of Athens it has been chosen to develop a thesis work about a displacement pump integrated into an ORC experimental unit.

Chapter 1

The pump in an Organic Rankine cycle

This chapter describe the influence of the pump in an Organic Rankine Cycle in terms of work and efficiency of the whole unit, the issues of the pump arise because of the usage of organic fluids and the different operating conditions compared to the conventional plants.

1.1 Why study the pump

To demonstrate the importance of the pump in an ORC plant, as it was done by Declaye in [3], is useful consider the Back Work Ratio that can be defined as the ratio of feed pump consumption over turbine production:

$$r_w = \frac{\dot{W}_{pp}}{\dot{W}_{tur}} \tag{1}$$

and considering also the temperature ratio:

$$r_T = \frac{(T_{ev} - T_{cond})}{(T_{crit} - T_{cond})} \tag{2}$$

in a simple subcritical Rankine Cycle with isobaric and isentropic transformations, without superheating and constant condensing temperature, the influence of the temperature ratio on the Back Work Ratio for some different fluids is showed in the figure 1. The trend is the same for all the fluids: the higher is the temperature ratio and the higher is the back work ratio. It is also clear how all the organic fluids have a higher back work ratio than the water and it is also different from one fluid to another, this is a first demonstration for how it is important to have an accurate model for the pump in a cycle different than a conventional one that uses water.

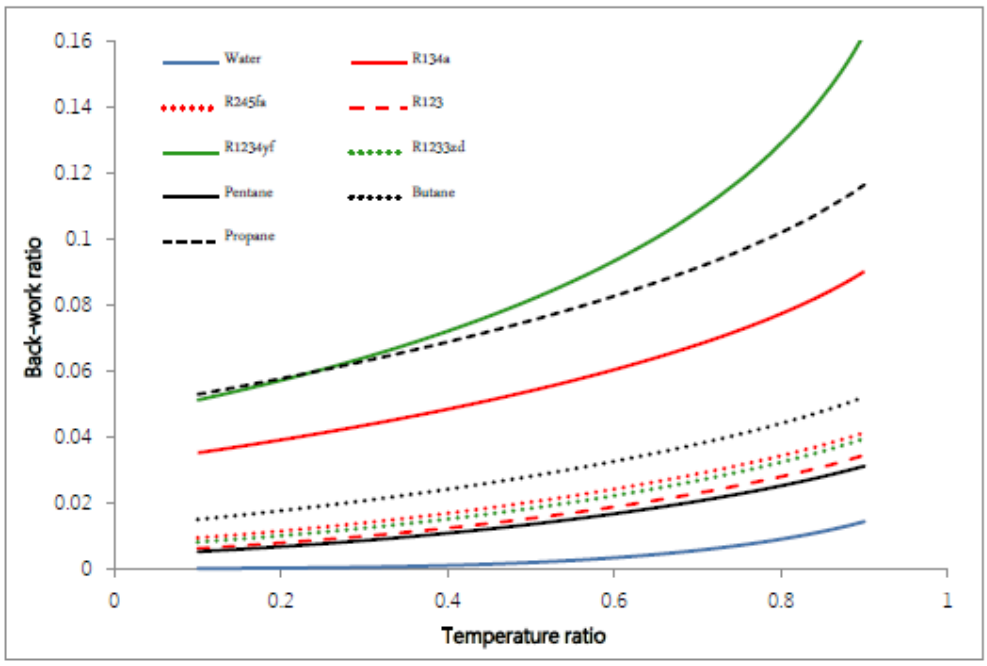

Figure 1: *Back-work ratio as a function of temperature ratio. From [3]*

For this kind of plant it is possible to compare the power of the pump for different fluids and considering two different pump global efficiency (100% and 50%), this analysis was done by Declaye in [3]. From the figure 2. we can see how the pump's impact is more important with organic fluids.

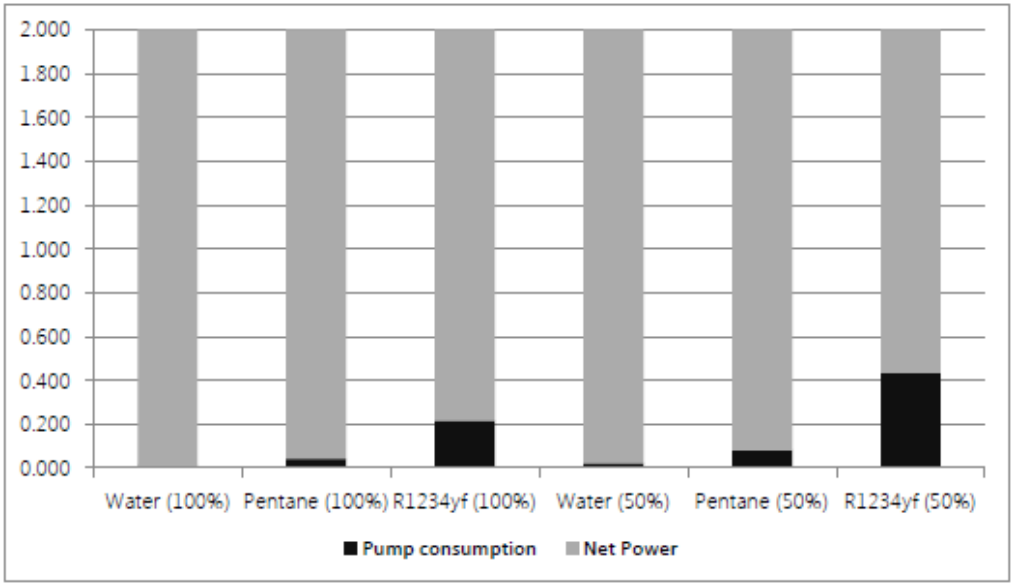

Figure 2: *Net power and feed pump power for three different fluid for two different pump efficiency. From [3]*

Considering also the back work ratio with some approximations:

$$\frac{\dot{W}_{pp}}{\dot{W}_{tur}} = \frac{V_{flow,pp}(p_{ev} - p_{cond})}{V_{flow,tur}(p_{ev} - p_{cond})} = \frac{\dot{m}}{\rho_{pp}} \frac{\rho_{inl,tur}}{\dot{m}} = \frac{\rho_{inl,tur}}{\rho_{pp}} \quad (3)$$

Where, p_{ev} is the evaporating pressure, p_{cond} is the condensing pressure, $\dot{m}$ is the mass flow rate of working fluid, ρ_{pp} is the fluid density at the pump inlet and $\rho_{inl,tur}$ is the fluid density at the turbine inlet. So the higher the density variation from pump inlet to turbine inlet the lower the back work ratio. For water, the density is reduced by a factor 3400 while the fluid changes from saturated liquid at 25°C to saturated vapour at 80°C. For organic fluids, the variation of density is much more limited. For instance, for the same temperature and phase change, the density reduction factor is only 61 and 6 for n-pentane and R1234yf respectively, as described in [3].
From other studies (Lin [13]) it is resulted that the efficiency variation of the 7 different pumps from 31% to 81% has comported a variation of the ORC thermal efficiency from 7.1% to 9.2%.

1.1.1 Impact of cavitation in ORC plant

The cavitation is a big problem in the pump system, it is the formation of vapour bubbles of the fluid at the inlet suction, where the pressure is minimum and is lower than the vapour pressure at the temperature of the fluid.
This phenomenon causes an increase of vibration and noise level, drop of delivered flow rate and/or pressure head, efficiency drop and pump damage due to cycle implosion of vapour bubble.
All of this is caused from:

- Pressure drop in piping or other elements (filter, heat exchanger, etc) located in the pump inlet line;
- The acceleration of the fluid in the vicinity of the pump rotor;
- In volumetric pumps, the pressure drop needed for the fluid to enter the machine;
- An increase of the saturation pressure due an increase of the fluid temperature.

To avoid this phenomenon it is important keep the pressure of the fluid always higher than the pressure of vapour.

The difference between the fluid and the saturation pressure is called NPSH available:

$$NPSHa = \frac{p_{res}}{\rho g} + H - \frac{\Delta p_{res,pp}}{\rho g} - \frac{p_{sat}}{\rho g} \quad (4)$$

Where:

p_{res} = pressure in the reservoir located at the condenser outlet

H = altitude difference between the fluid reservoir and the pump

$\Delta p_{res,pp}$ = pressure drop between the fluid reservoir and the pump

p_{sat} = saturation pressure

ρ = fluid density

g = gravitational constant

The pump manufacturer provide the limit value for the NPSH to avoid the cavitation:

$$NPSHa > NPSHr \quad (5)$$

Where NPSHr is the value provided by the pump manufacturer.

To increase the NPSHa the main measures are:

- Increase the pressure at the reservoir; it is possible introducing incondensable gas, but this solution has a bad impact on the other cycle transformations and then is not used.
- Increase the altitude difference between the reservoir and the pump suction; In some MW scale units, a several meters deep hole is drilled behind the ground and the pump is installed in that hole, but for KW units this solution is not economically convenient, so usually the reservoir is at the top of the plant and the pump at the bottom side with a distance like 1.5 meters.
- Reduce the pressure drop between the reservoir and the pump.
- Cooling down the liquid in order to reduce its saturation pressure; through a heat exchanger between the reservoir and the pump.

This last solution is the only one that can be really managed because the others have

limits. It is possible see, from analysis studies by Declaye in [3], how the subcooling impacts the cycle efficiency; considering a simple and ideal Rankine cycle with an organic fluid the result is showed in the figure 3.

It is clear that the subcooling is good for the cavitation because of the increase of the NPSHa, but from the point of view of the cycle is bad because of the decrease of the cycle efficiency.

Concludying, the NPSH of the pump should be as low as possible in order to limit the cycle efficiency reduction but enough to ensure stable operating condition without cavitation.

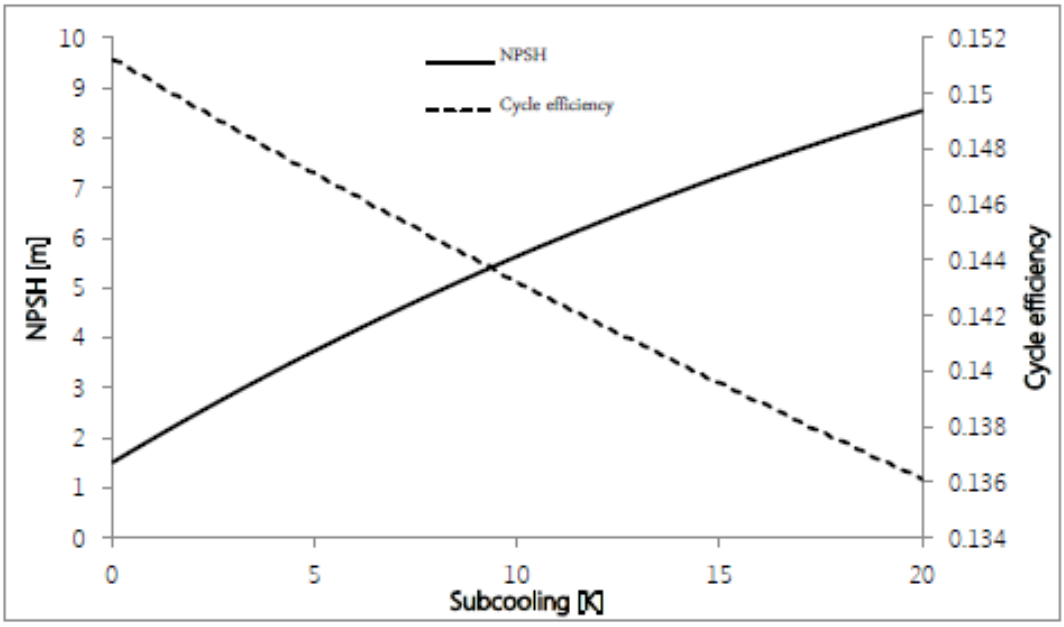

Figure 3: *Subcooling effect on the NPSH and cycle efficiency. From [3]*

All these issues just described find a strong justification for this work that has been developed following the same order of the follow chapters:

- characterization of the pump system in the ORC unit (chapter 2);
- modelling of the pump system (chapter 3);
- screening of the experimental data and calibration of the model (chapter 3);
- usage of the calibrated model to analyse the pump behaviour (chapter 4 & 5).

Chapter 2

The pump system

The chapter 2 describes the experimental equipment of the whole pump system integrated into the ORC unit, it is defined as pump system the set of the pump, the electric motor and the frequency driver.
The experimental unit is equipped of a multi-diaphragm pump because of its small size (some KW), considering also the conditions of low flow rate and high pressure head the volumetric pump is the best solution. Another reason of this choose are the losses of organic fluid which the cost and environmental impact are important, then the diaphragm pump is the best solution because has no leakages.
Diaphragm pumps are often used although the low efficiency because the organic fluid looses are very important.

2.1 The experimental unit

The National Technical University of Athens provide a micro ORC unit and in this paragraph is reported the description of the plant presented in the work *Experimental study on a low temperature ORC unit for onboard waste heat recovery from marine diesel engines* [7].
The marine ORC prototype unit is based on a conventional low-temperature subcritical Organic Rankine Cycle using R134a as working medium. This experimental unit has been designed as a waste heat recovery system for the jacket water of marine diesel auxiliary internal combustion engines (ICEs). In order to simulate the operating characteristics of such engines, the heat input is in the order of 90kWth at a low-temperature (90°C), and is supplied by a natural gas boiler via an intermediate plate heat exchanger (evaporator). The boiler thermal output is

adjustable and thus part load operation can be simulated as well. A schematic diagram of the unit is presented in Figure 4.

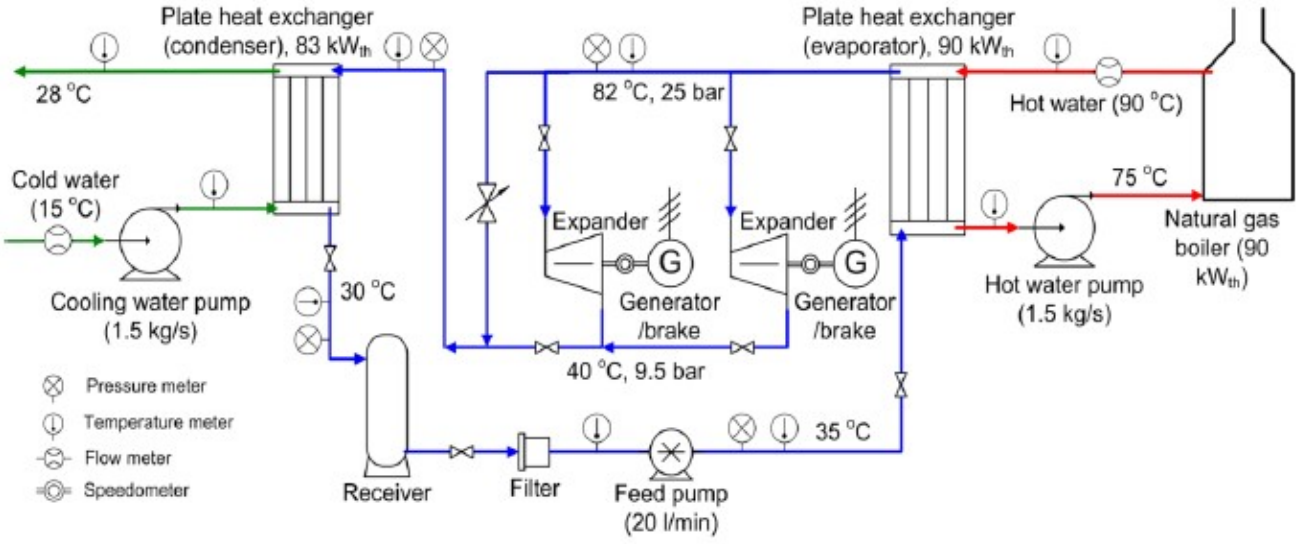

Figure 4: *Schematic diagram of the ORC prototype unit. From [7]*

The cycle is fed by a receiver (feed tank) at an average pressure of 9.5 bar and an average temperature of 30 °C. These parameters are controlled by the cold water flow in the condenser, which is adjusted by a regulatory valve. The feed pump is a positive displacement multi-diaphragm pump that subsequently raises the pressure of the fluid at about 22-25 bar, depending on the operational conditions, and leads it to the evaporator. At a nominal speed of 960rpm a flow rate of 20lt/min is achieved. The rotational speed of the pump is controlled by a frequency drive. As a result, the refrigerant mass flow rate can be adjusted according to the unit load and the desired superheating temperature of the vapour, given the fact that the delivered volume flow rate of diaphragm pumps is in most cases a linear function of their rotational speed. The high pressure vapour is expanded in two parallel scroll expanders, while a by-pass section controlled by an electromagnetic valve can alternatively lead the flow directly to the condenser. Each scroll expander drives an asynchronous motor/generator through a 1:1 belt drive, which can be coupled and uncoupled by an electromagnetic clutch. Both generators are connected to the 50Hz/400V electrical

grid via a regenerative inverter module, which provides both grid stability and rotational speed control of the generators and hence of the expanders. For a given pump rotational speed (and thus mass flow rate), the inlet pressure of the scroll expanders is directly adjusted by their rotational speed, since the processed mass flow rate for volumetric machines is given by the product of the inlet density (ρ_{inl}) multiplied by the swept volume (V_H) and the rotational speed (N) of the machine (eq.6).

$$\dot{m} = \rho_{inl} \cdot V_H \cdot N \tag{6}$$

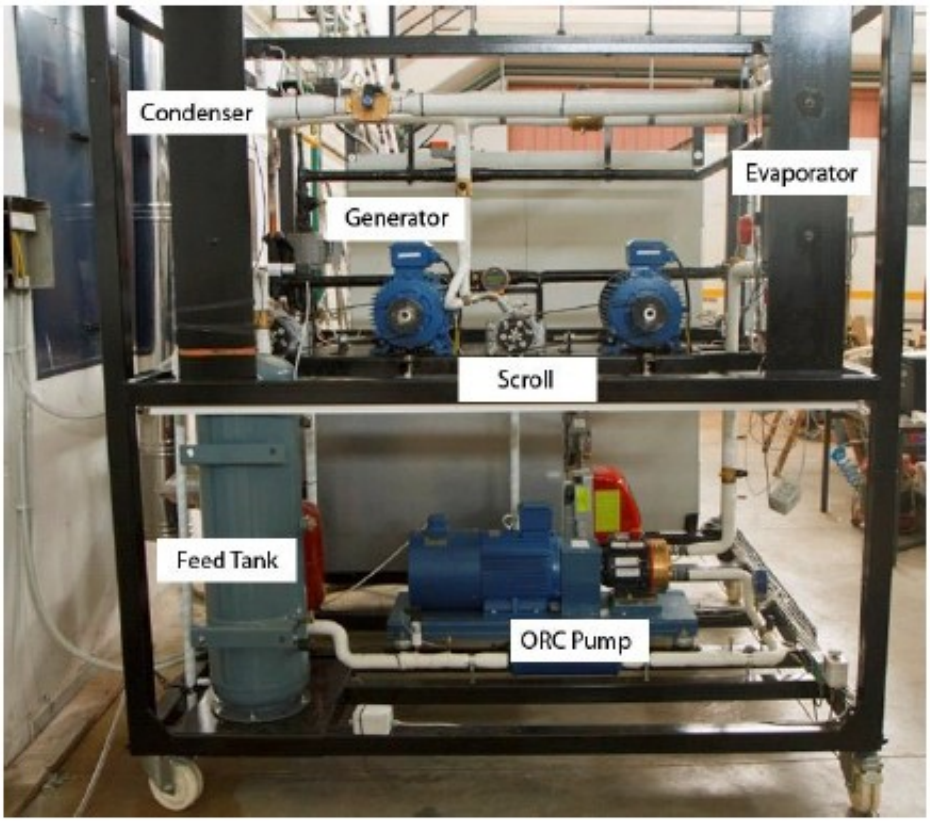

Figure 5: *ORC experimental unit. From [7]*

An increase (decrease) of the rotational speed allows for a decrease (increase) of the density of the refrigerant at the expander inlet and thus causes a decrease (increase) of the respective inlet pressure. Finally, the expanded vapour is led to the condenser (plate heat exchanger), the condensate returns to the feed tank, and the cycle starts

over. The ORC unit (Figure 5.) produces 5 kWel of net electrical power, at a design cycle pressure of 25bar and a temperature of 82°C.
Various instruments have been mounted at all key-points of the cycle, in order to evaluate the performance of the different components of the ORC unit.
Thermocouples and pressure transducers record the thermodynamic procedure; an electromagnetic flow-meter supervises the hot water volume flow rate and two tachometers the scrolls actual rotational speed. All important parameters regarding the electrical motors of both the pump and the generators, such as the consumed/produced active power are retrieved by the respective frequency drives.

2.1.1 The diaphragm pump

The diaphragm pump has two cavities, one with oil and one with the working fluid. These cavities are separated by a flexible membrane and in the oil cavity there is a movable piston that allows to deform the membrane.
Because of the deformation of the membrane the working fluid can flow trough the other cavity, inlet and outlet valves are necessary.

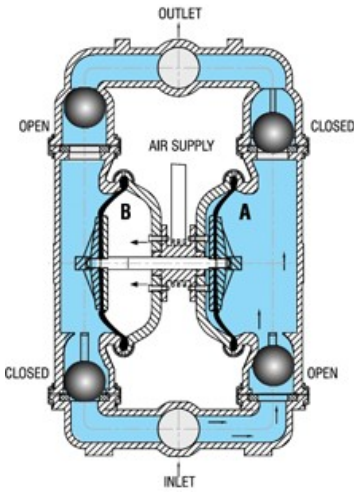

Figure 6: *Multi-diaphragm pump operating scheme.*

The configuration of a diaphragm pump allows isolating the mobile parts of the pump from the working fluid. Therefore, no dynamic sealing is required on the working

fluid side.

There are also multi-diaphragm pump that are using the same principle of the single diaphragm pump but there are several membranes in parallel. The flow rate from a multi-diaphragm pump is more stable.

2.1.2 Datasheet of the pump

Are reported in this subparagraph the specifications data of the used pump.

D/G-10 Dimensions

Models with Metallic Pumping Head

Brass

Cast Iron

316 Stainless Steel

Nickel Alloy (C Series)

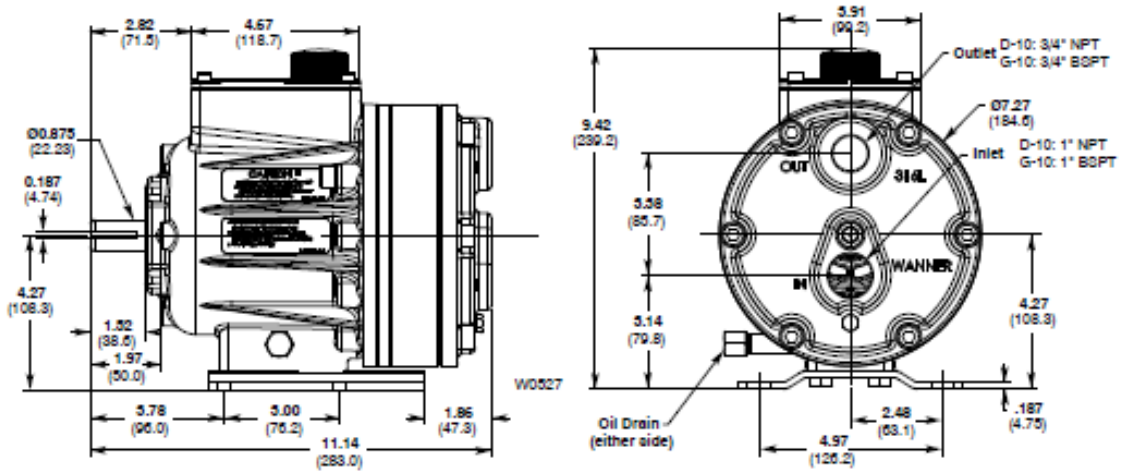

Figure 7: *Dimensions of the pump, from Hydra-Cell datasheet.*

D/G-10 Specifications

Max Pressure	Metallic: 1000 psi (70 bar) Non-Metallic: 250 psi (17 bar) Slurry Duty (SD): 300 psi (21 bar)		
Capacity @ Max Pressure			
	rpm	gpm	l/min
D/G-10-X	1450	7.8	29.0
D/G-10-E	1750	8.0	30.3
D/G-10-S	1750	6.0	22.7
D/G-10-I	1750	3.9	14.9
Delivery @ Max Pressure			
	revs/gal		revs/liter
D/G-10-X	185		50
D/G-10-E	219		58
D/G-10-S	292		77
D/G-10-I	448		117
Max Inlet Pressure			
Metallic:	250 psi (17 bar)		
Non-Metallic:	50 psi (3.5 bar)		
Slurry Duty (SD):	50 psi (3.5 bar)		
Max Temperature			
Metallic:	250°F (121°C) – consult factory for temperatures above 160°F (71°C)		
Non-Metallic:	Polypropylene: 120°F (49°C); Kynar, Celcon & Slurry Duty: 140°F (60°C) – consult factory for temperatures above 120°F (49°C)		
Inlet Port	D-10: 1 inch NPT G-10: 1 inch BSPT		
Discharge Port	D-10: 3/4 inch NPT G-10: 3/4 inch BSPT		
Shaft Diameter	7/8 inch (22.22 mm)		
Shaft Rotation	Bidirectional		
Bearings	Tapered roller		
Oil Capacity	1.1 US quarts (1.05 liters)		
Weight	Metallic Heads: 48 lbs (22 kg) Non-Metallic Heads: 35 lbs (16 kg)		

Calculating Required Horsepower (kW)*

$$\frac{15 \times \text{rpm}}{63{,}000} + \frac{\text{gpm} \times \text{psi}}{1{,}460} = \text{electric motor HP*}$$

$$\frac{15 \times \text{rpm}}{84{,}428} + \frac{\text{lpm} \times \text{bar}}{511} = \text{electric motor kW*}$$

* rpm equals pump shaft rpm. HP/kW is required application power. Use caution when sizing motors with variable speed drives.

Figure 8: *Specifications of the pump from hydra-Cell datasheet.*

2.1.3 The electric motor

The data of the manufacturer of the electric motor are shown in this subparagraph.

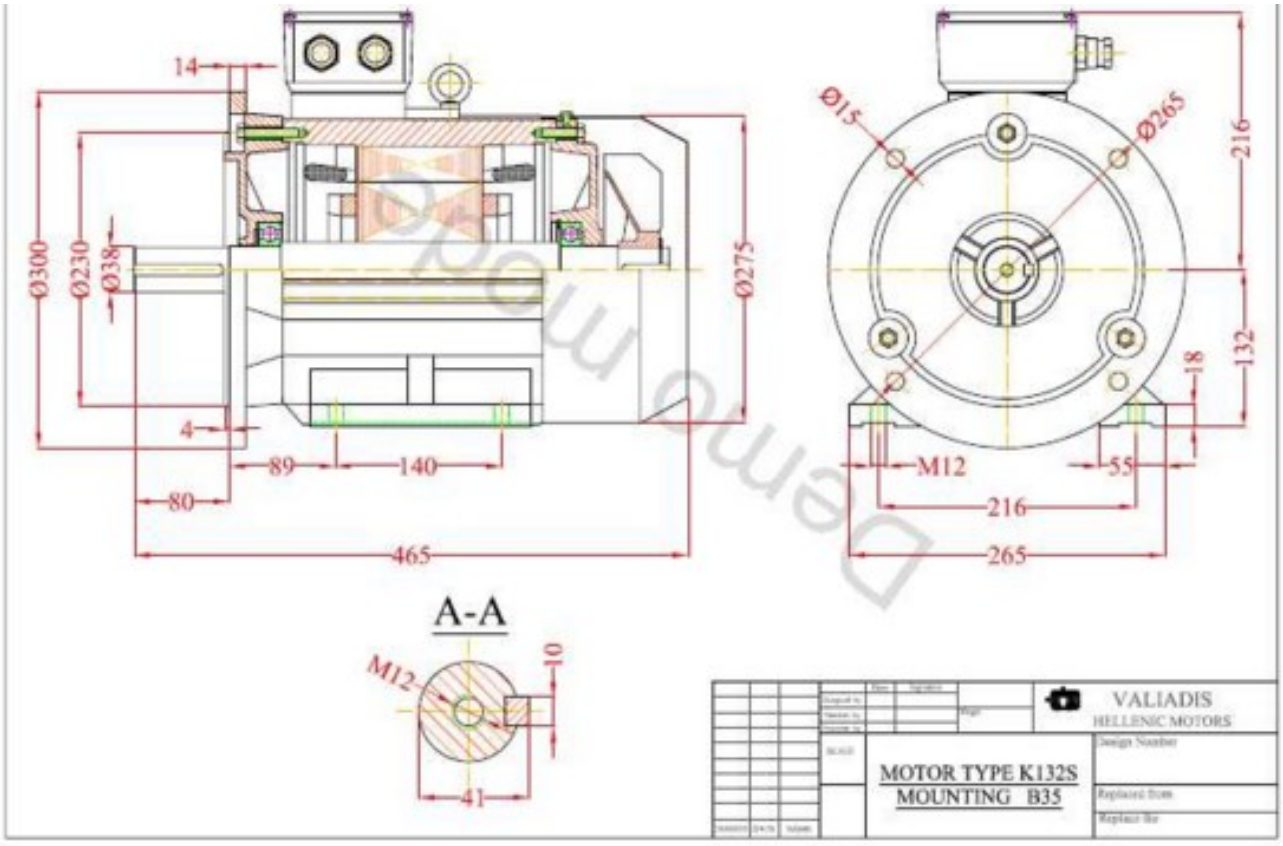

Manufacturer	**VALIADIS**	Power factor	**0.76 PF FL**
Family / Frame	**K132S**	Efficiency FL	**86.40**
Rated / Power	**3.00 kW / 4.00 hp**	Torque FL	**30**
Speed	**960 RPM**	Locked rotor torque/full load torque	**2.10**
Mounting	**B35**	Star delta torque/full load torque	**Y-MOTOR**
Voltage / Connection	**230-Δ / 400-Y**	Pull out torque/full load torque	**3.20**
Frequency	**50 Hz**	Star delta pull out torque/full load torque	**Y-MOTOR**
Enclosure	**55 IP**	Locked rotor current/full load current	**6.4**
Full load current	**6.60 A / 11.43 A**	Star delta locked current/full load current	**Y-MOTOR**
Insulation class	**F**	Bearing DE	**6208ZZC3**
Comment	**3x PTC 150 °C**	Bearing NDE	**6208ZZC3**
Feature	**cast iron - motor**		
Weight	**63.0**		

Figure 9: *Manufacturer specifications of the electric motor, from Valiadis S.A. datasheet.*

From the manufacturer test it is possible interpolate a performance curve that as described in the next chapter is used in the pump model.

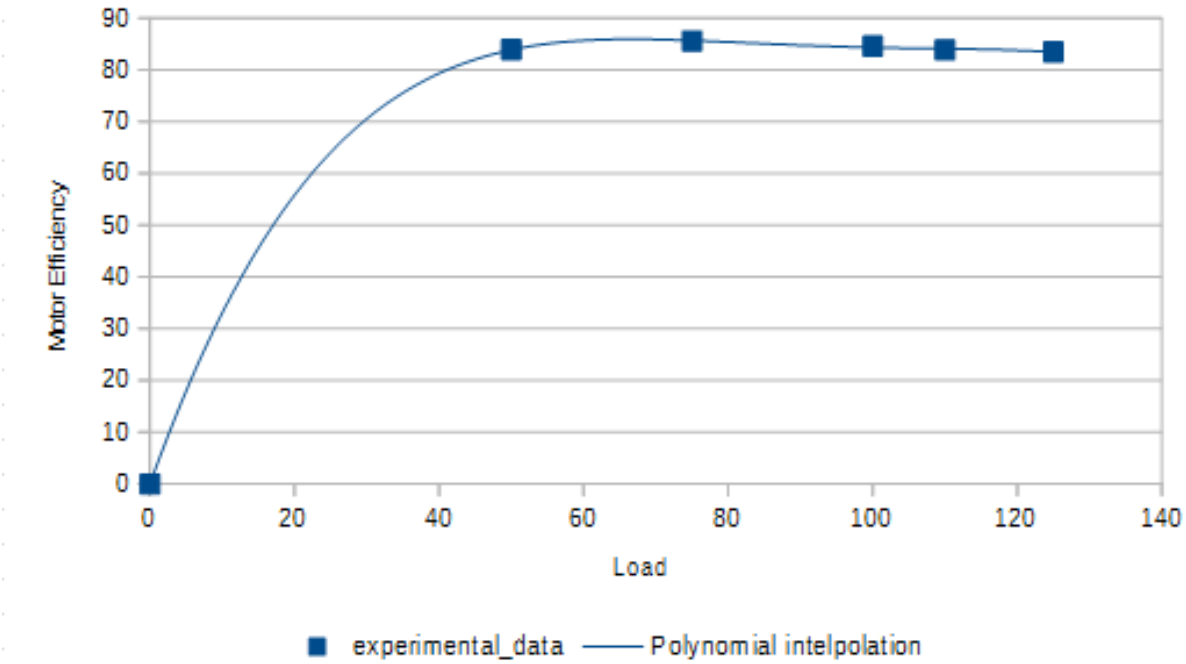

Figure 10: *Interpolation of the experimental data of the electric motor.*

2.2 The pump system concept

In this paragraph it is explained how is modelled the energy that flow trough the pump system described before.

The energy from the grid comes to the frequency driver (VSD, variable speed driver) $\dot{W}_{el}$ and go trough the motor, but a little part of this energy is wasted in heat $Q_{los,vsd}$. Also in the motor the are losses, mechanic and electric, that are dissipated as heat in the environment $Q_{los,mot}$. The electric work is transformed in mechanic work ($\dot{W}_{mech}$) and is delivered at the pump trough the hub, at the end in the pump there are other losses that are dissipated as heat at the environment $Q_{los,pp}$ or as a fictive heat of the working fluid ($Q_{los,flu}$). Heat exchange between fluid, pump and environment is also permitted (Q_{hex}). Figure 11. show this chain.

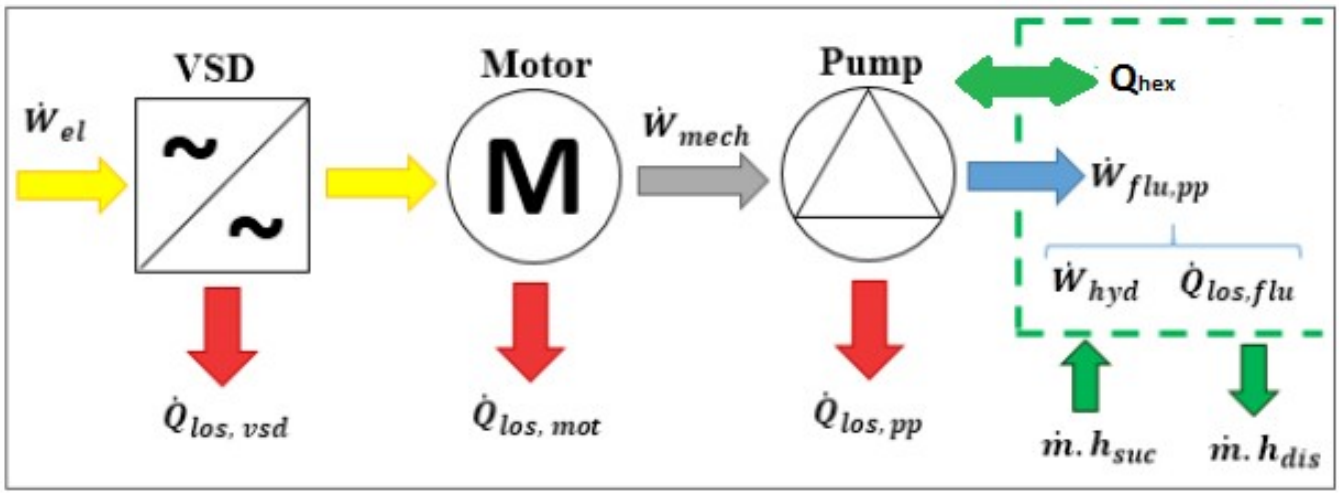

Figure 11: *Energetic conceptual scheme of the pump. From [6] without the adiabatic assumption.*

As said before, inside the pump, without consider the motor and the frequency driver, there are different kind of losses that can be divided in:

Hydraulic losses

The flow in the pump is subjected to numerous disturbances which create irreversibilities in the pumping process. They include internal leakages, friction between the fluid and the pump parts, pressure drops through the admission and exhaust ports, etc.

Mechanical losses

A fraction of the power delivered to the pump shaft by the motor is not converted into hydraulic power. This fraction is dissipated, under the form of heat, into mechanical parts subject to friction such as seals and bearings.

Chapter 3

The semi-empirical model and its calibration

To study the behaviour of the pump and also predict it a semi-empirical model in steady-state conditions was chosen. Semi-empirical model is a good compromise between the computational complexity of a deterministic model and the necessity of data from manufacturer and the experimental unit of the empirical model (figure 12.). This model consist in a zero-dimensional model that needs some experimental data from the unit and the calibration of fictitious parameters that are geometrical and operational. The model follow the same concept of the volumetric expander models developed in others research but with the adequate measures for the pump, changing the operational parameters.

The model is built in EES environment exploiting the fluids package and the minimization function to calibrate the model. After the calibration this EES model can implemented in another EES script that includes all the ORC components.

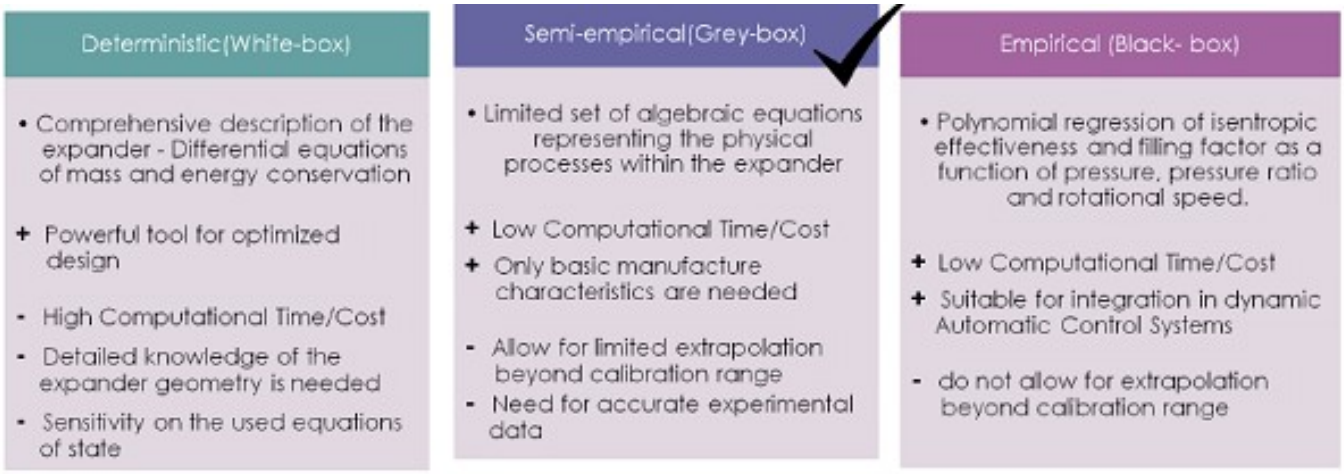

Figure 12: *Differences between the different models. From [8]*

3.1 The methodology

The methodology used for the calibration of the model consist in an optimization problem, independent parameters (x_i) are chosen to minimize a defined function ($f(x_i)$). It is necessary use this methodology because the unknowns are more than the equations and the problem can not be solved.

As said before the model is a zero-dimensional model built in EES environment, it consists in a set of thermodynamic and semi-empirical equations chosen according to the works in literature. In this model the independent parameters come from the semi-empirical equations and the design of the machine, the function that has to be minimized is the error between the model results and the experimental data.

The model use the experimental data come from the ORC unit to try to fit them in the same operating conditions that are measured, so they are used as inputs.

In figure 13. there is a schematic interpretations of this method.

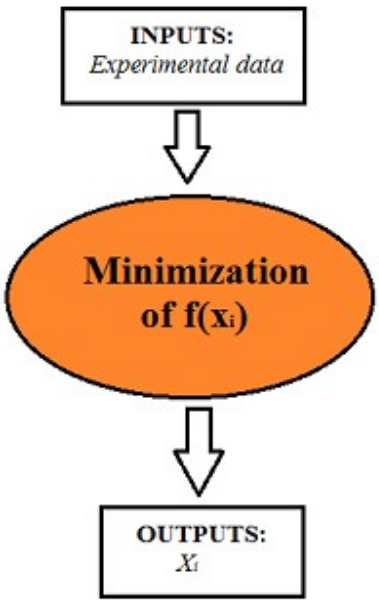

Figure 13: *Calibration and analysis for a pump operating condition.*

3.2 General view of the semi-empirical model

This model is inspired according to the model proposed by EXP-HEAT [8] for a piston expander and also used in other research, like V.Lemort et al.[1] for the modelling of Scroll expanders and Winandy [14] for the open drive reciprocating compressor. It is reminded that a semi-empirical model consists of a set of parameters which require to be calibrated with experimental results in order to simulate an actual operating machine.

The pump is modelled as a sequence of thermodynamic transformations, these are:

1. **$su_0 \rightarrow su$: Adiabatic mixing of main ad leakage flow.** A little part of the working fluid in the high pressure section goes toward the low pressure section through the tightness.
2. **$su \rightarrow su_1$: Adiabatic supply pressure drop.** Due to friction losses at the inlet valves.
3. **$su_1 \rightarrow su_2$: Adiabatic mixing of main and trapped flow.** A part of the working fluid remains inside the pump because can not expel all the flow due the mechanical tolerances (dead volume).
4. **$su_2 \rightarrow su_3$: Isobaric supply heat exchange.** Due to different temperature between the fluid and the machine.
5. **$su_3 \rightarrow ad$: Adiabatic isentropic compression.**
6. **$ad \rightarrow ex$: Isochoric adiabatic expansion/compression.** Can be that the fluid has a pressure different than the system pressure (opening of the discharge valve).
7. **$ex \rightarrow ex_1$: Isobaric exhaust heat exchange.** Due to different temperature between the fluid and the machine.
8. **$ex_1 \rightarrow ex_2$: Adiabatic exhaust pressure drop.** Due to friction losses at the outlet valves.
9. **$ex_1 \rightarrow 0$: Adiabatic isentropic expansion of the trapped mass flow.** The trapped mass flow has an expansion due to the return stroke of the piston.

10. **0 → 1 : Isochoric adiabatic expansion/compression.** Can be that the trapped mass flow has a different pressure than the pressure of the supply line (opening of the suction valve).
11. **ex → L : Adiabatic leakage pressure drop.** To adapt the pressure of the leakage to the suction pressure.

Figure 14. shows the whole process.

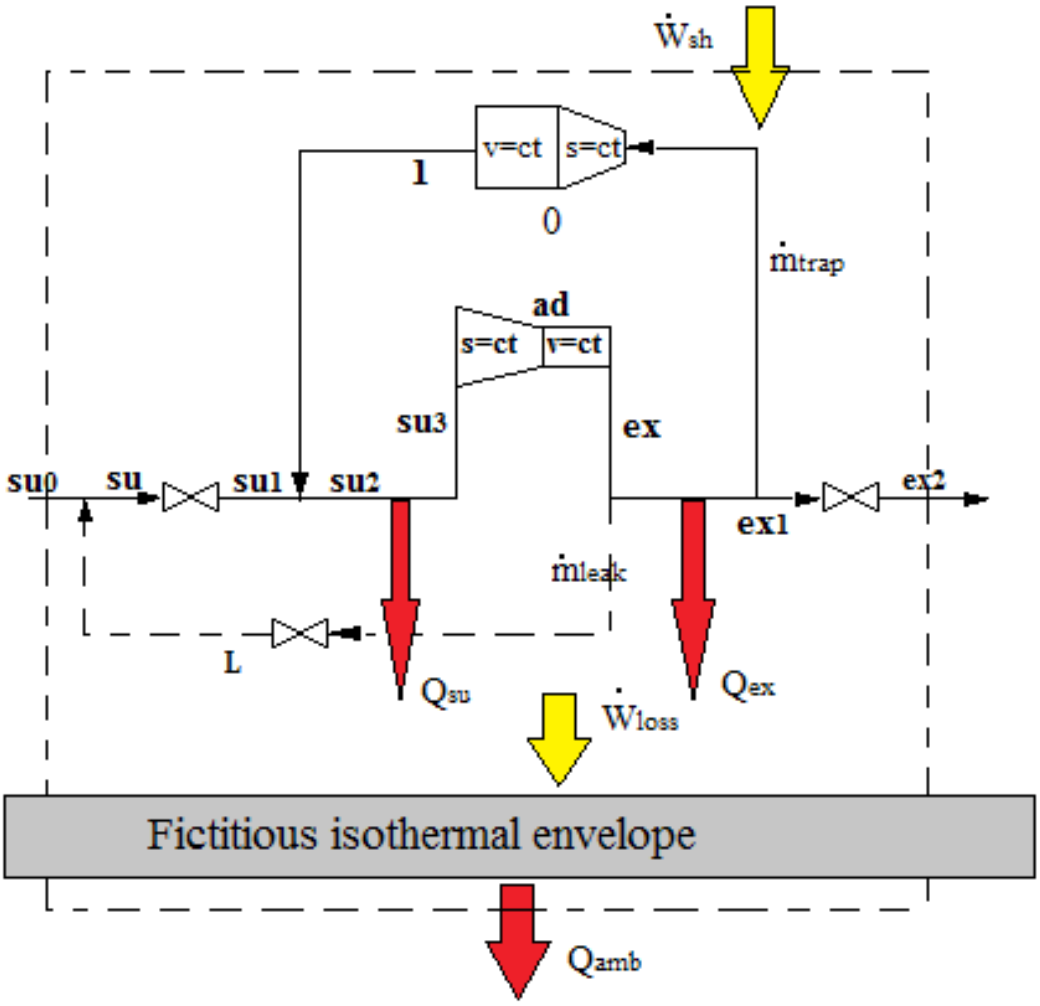

Figure 14: *Thermodynamic scheme of the pump.*

3.2.1 Geometrical parameters

This paragraph talk about the geometrical parameters of the pump, these are useful to take into account the valves timing and others geometrical imperfections, like the dead volume, that are indispensable for a good operation of the pump.

This method is used also for the reciprocating expander in [8,4] and to adapt the parameters at the diaphragm pump some of these are modified because of the different operation cycle.

- **The total volume V_s.** Is the total volume of the working fluid chamber when the piston and the membrane are in upper position, the valves are both closed and the compression is next to start (su_3). For a multi-diaphragm machine it represent the total volume of the machine. (figure 15.)

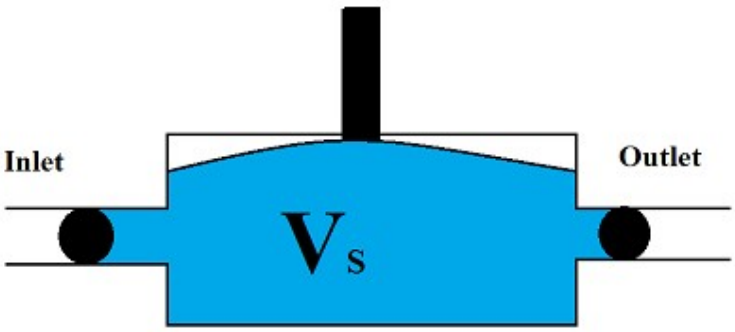

Figure 15: *Total volume.*

- **The dead volume V_0.** Is the volume left when the piston and the membrane are at the bottom position and the valves are both closed (ex_1). This volume is the reason of the trapped fluid. (figure 16.)

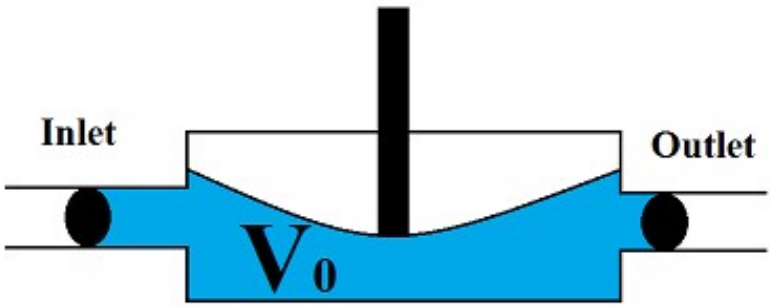

Figure 16: *Dead volume.*

- **The swept volume V_H.** Is the volume swept by the membrane during its movement. For a multi-membrane machine it represents the total swept volume of the machine. (figure 17.)

  This geometrical parameter gives a quick measure of the delivered mass flow and considering the total and dead volume it is equal to their difference:

$$V_H = V_s - V_0 \tag{7}$$

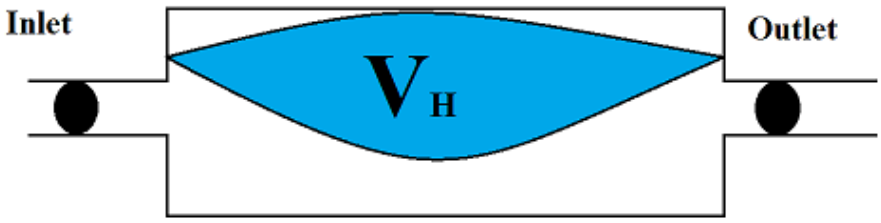

Figure 17: *Swept volume.*

- **The ratio** $C = \frac{V_0}{V_s}$ **.**

- **The ratio** $f_a = \frac{V_1}{V_s}$ **.** Where V_1 is the chamber volume when the inlet valve open and the suction phase begins (after the transformation number 10). The ratio f_a is directly linked with the mass flow that enters the pump. As it rises, the inlet valve remain close for longer time and the processed mass flow is reduced, it will be higher also the expansion of the trapped mass flow and so can produce vapour. The longer is the expansion and the grater is the specific volume of the trapped mass, as a consequence the available volume for the inlet mass flow is lower. This ratio should be as low as possible to avoid the formation of vapour and a huge expansion of the trapped fluid, but is not possible avoid it because of the return stroke of the piston. (figure 18.)

  The parameter f_a is modified respect the one used in the expander model, in the pump cycle is considered the time of opening of the valve instead of the

closing.

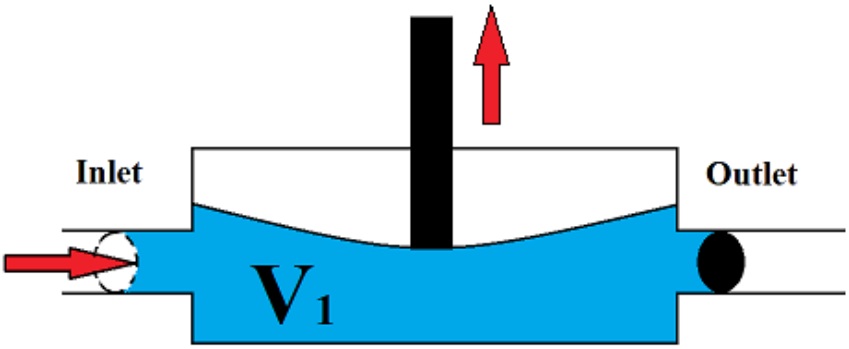

Figure 18: *Volume V_1.*

- **The ratio** $f_p = \frac{V_{ex}}{V_s}$ **.** Where V_{ex} is the chamber volume when the outlet valve open and the discharge phase begins (ex). This parameter is equal at the ratio of the specific volume before and after the isentropic compression ($su_3 \rightarrow ad$) because the flow rate does not change during this transformations.
  So the higher the ratio the higher the compression. This parameter should be such that at the end of the compression the pressure is close at the required pressure by the circuit for all operating conditions. As the previous parameter also this is modified considering the time of opening of the valve (figure 19.)

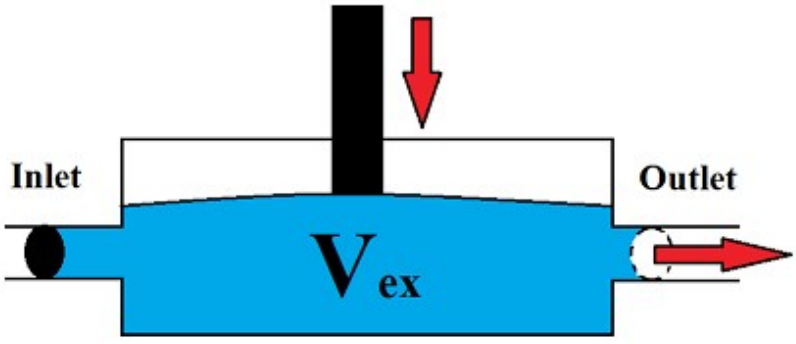

Figure 19: *Volume V_{ex}.*

It is also introduced a new parameter that is the ratio between f_a and C (equation 8.). It is called f_E and is also equal at the ratio between the specific volume after and before the expansion.

$$f_E = \frac{f_a}{C} = \frac{V_1}{V_0} = \frac{v_1}{v_{ex1}} \tag{8}$$

In function of this parameter after the expansion of the trapped fluid there is a isochoric expansion or compression, it is analogous to f_p in the compression phase. In figure 20. it is showed in a p-V diagram the sequence of the thermodynamic transformations of the pump, this is a qualitative diagram.

Due to dead volume (V_0) there is fluid trapped in the pump that after the expansion go to occupy a volume (f_a*V_s) bigger than V_o and because of that the pump can not suck a mass flow proportional to the entire volume V_s.

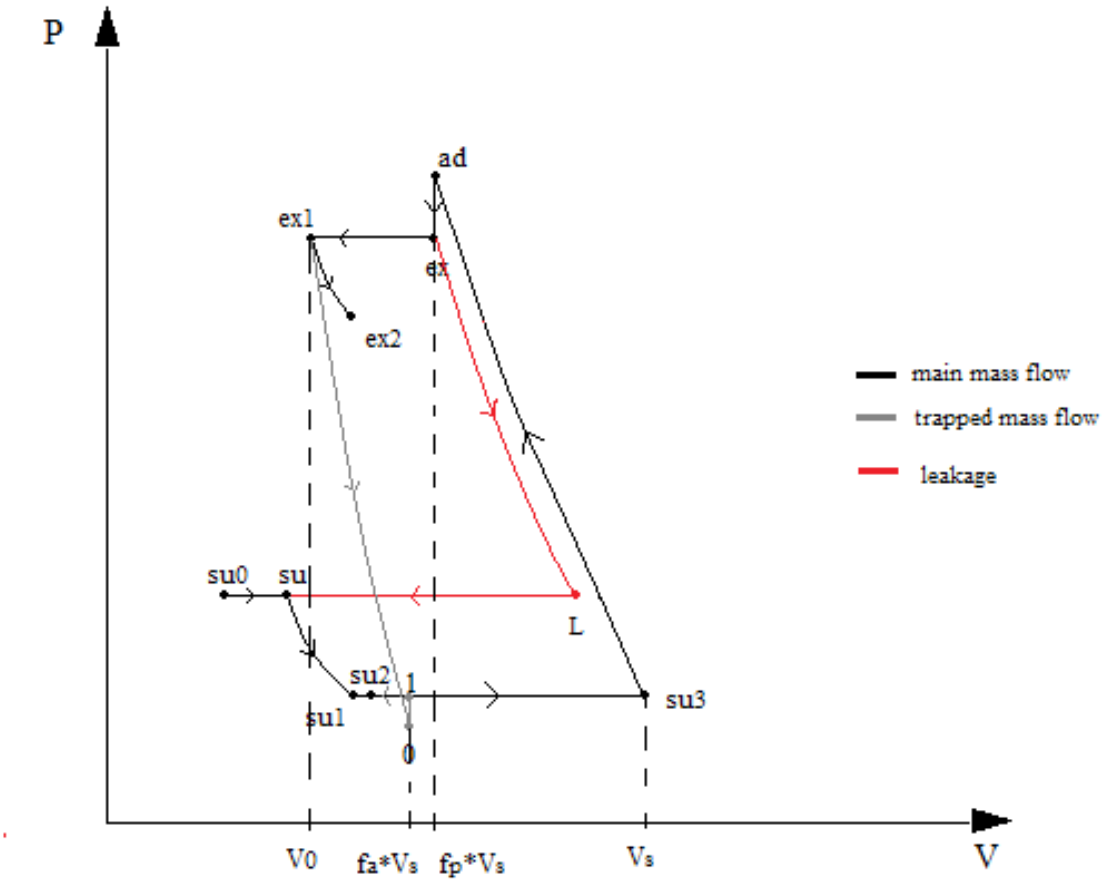

Figure 20: *p-V diagram of the pump.*

3.2.2 Under and over compression

Under-compression occurs when the internal pressure ratio imposed by the pump (p_{ad}/p_{su3}) is lower than the system pressure ratio (p_{ex}/p_{su3}). In that case, the pressure in the pump chambers at the end of the compression process (p_{ad}) is lower than the pressure in the discharge line plus the discharge pressure drop. The modelling assumes that there is no pressure drop through the discharge port. In order to equalize the pressures in the discharge chambers and in the discharge line, some fluid ($\Delta\dot{m}$ in eq.9) has to flow in of the discharge chambers. The modelling assumes it is achieved instantaneously as soon as the pump chambers open onto the discharge line. The energy balance over the discharge chamber can be expressed as follows:

$$(\dot{m}_{ad}+\Delta\dot{m})u_{ex}-\dot{m}_{ad}\cdot u_{ad}=\Delta\dot{m}\cdot h_{ex} \qquad (9)$$

In this case $\Delta\dot{m}$ come inside the chambers and the discharge work it will be greater.

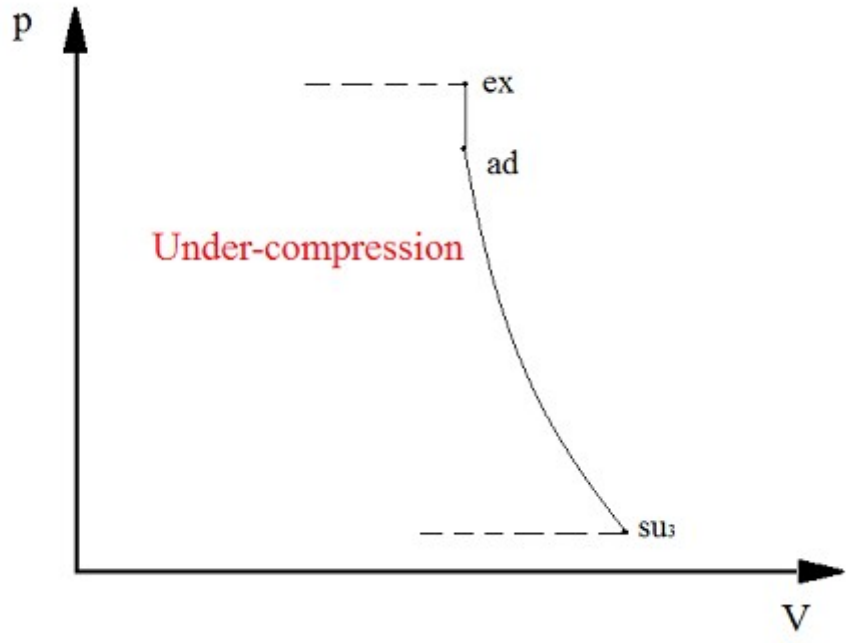

Figure 21: *Example of under-compression after the transformation $su_3 \rightarrow ad$.*

Over-compression occurs when the internal pressure ratio imposed by the pump is higher than the system pressure ratio. Here the fluid $\Delta\dot{m}$ (eq.10) flow out of the discharge chambers spontaneously and the discharge work it will be lower.

The energy balance over the discharge chamber is:

$$(\dot{m}_{ad}-\Delta\dot{m})u_{ex}-\dot{m}_{ad}\cdot u_{ad}=-\Delta\dot{m}\cdot h_{ex} \tag{10}$$

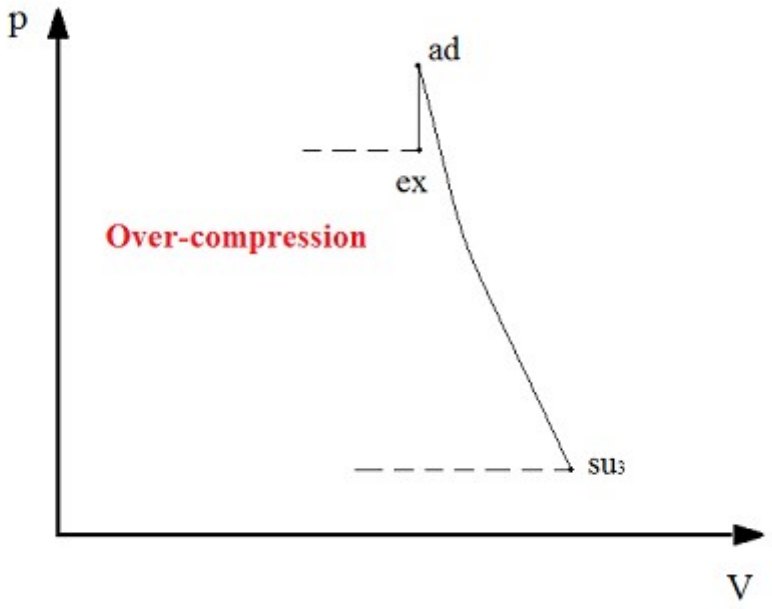

Figure 22: *Example of over-compression after the transformation $su_3 \rightarrow ad$.*

There is no work directly associated to the under- and over-compression throttling. The discharge work has to be increased or decreased in function of the under or over-compression, but this term of the work is neglected in the semi-empirical model because the its low value.

The description of the over- and under-compression done is for the transformation ad→ex but is also valid for the transformation 0→1.

This method is proposed by Quoilin *et al.* [1], used also in others articles [4,8] and is adapted at the pump cycle in this work.

3.5 Analysis of the model components

I. Inlet mass flow rate

The inlet mass flow rate is calculated considering the trapped fluid at the end of the isentropic expansion and the leakages, because they are already inside the chamber volume during the suction phase:

$$\dot{m}_{inl} = \frac{N}{60}\left(\frac{V_s}{v_{su3}} - \frac{f_a \cdot V_s}{v_1}\right) - \dot{m}_{leak} \tag{11}$$

It is followed the same concept of [4,8] but using the pump geometrical parameters and considering differently the behaviour of the leakages.

The total mass flow that is worked by the pump is:

$$\dot{m}_{tot} = \dot{m}_{inl} + \dot{m}_{trap} + \dot{m}_{leak} \tag{12}$$

Where $\dot{m}_{trap}$ and $\dot{m}_{leak}$ are the mass flow rate trapped and from the leakages respectively.

II. Adiabatic mixing between main and leakage flow ($su_0 \rightarrow su$)

This process is adiabatic and isobaric, the equations are:

$$\dot{m}_{su0} \cdot h_{su0} + \dot{m}_{leak} \cdot h_L = \dot{m}_{su} \cdot h_{su} \tag{13}$$

$$\dot{m}_{su} = \dot{m}_{su0} + \dot{m}_{leak} \tag{14}$$

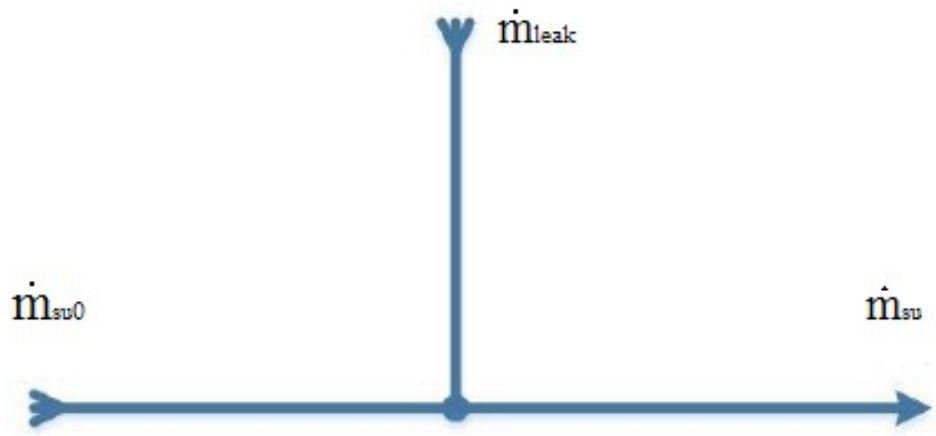

Figure 23: *Adiabatic mixing between main and leakage flow.*

III. Adiabatic supply pressure drop ($su \rightarrow su_1$)

The supply pressure drop is modelled as an isentropic flow in a simple nozzle. The fluid can be also considered incompressible due to the liquid state and the low pressure drop.

This method is used also in [3,8].

Figure 24: *Adiabatic supply pressure drop.*

The area A_{su} is a fictitious area that simulates the procedure of the pressure drops in the current machine. This parameter is determined from experimental data, using the model calibration process that will be presented in the next chapter.

From the momentum conservation equation for adiabatic flow and the previous assumptions it is possible calculate the pressure drop:

$$\Delta p_{su} = \frac{1}{2} \frac{\dot{m}_{su\,1}^2 \cdot v_{su}}{A_{su}^2} \tag{15}$$

IV. Adiabatic mixing of main and trapped flow ($su_1 \rightarrow su_2$)

As the adiabatic mixing showed before.

V. Isobaric supply heat exchange ($su_2 \rightarrow su_3$)

Due to the fact that the pump shell is hotter than the working fluid there is heat

transfer from the shell to the fluid as showed in figure 25.

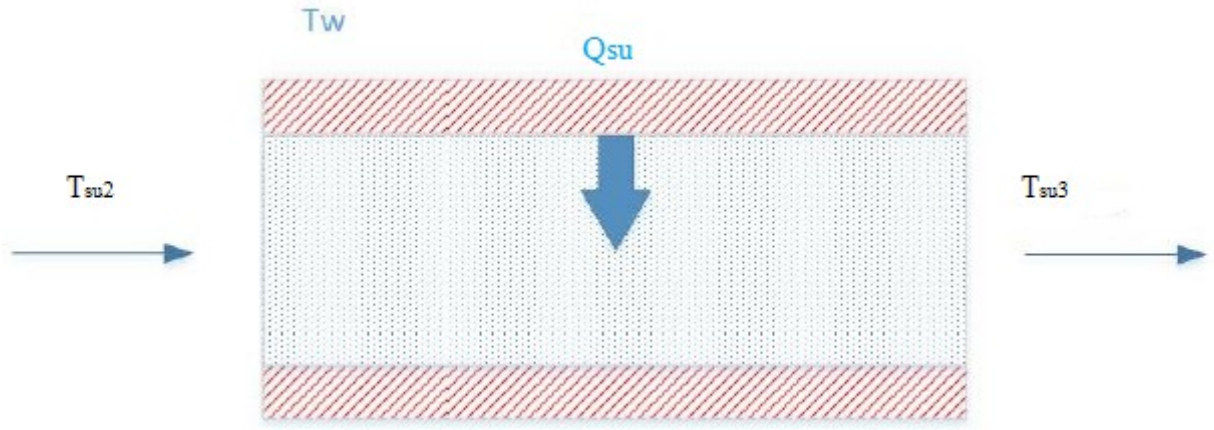

Figure 25: *Isobaric supply heating.*

Where T_w in the figure is the shell temperature.

This process is modelled with thermodynamic equations and the ε-NTU method:

$$Q_{su} = \dot{m}_{su3}(h_{su3} - h_{su2}) \tag{16}$$

$$Q_{su} = (1 - e^{\frac{-AU_{su}}{\dot{C}_{su2}}})\dot{C}_{su2}(T_w - T_{su2}) \tag{17}$$

$$AU_{su} = AU_{su,nom}\left(\frac{\dot{m}_{inl}}{\dot{m}_{nom}}\right)^{0.8} \tag{18}$$

Where AU_{su} is the heat transfer coefficient and depend of the mass flow rate, while $\dot{m}_{nom}$ is the nominal mass flow rate (0.39 kg/s).

The nominal heat transfer coefficient ($AU_{su,nom}$) has to be calibrated. The equation 18. can be justified by the Reynolds' analogy for a turbulent flow through a pipe by assuming that the fluid properties, not included in this expression, remain unchanged. The value of the AU_{su} depends on the mass flow rate of the working fluid and is given by Equation (18) proposed by Lemort *et al.* [1].

V. Adiabatic and isentropic compression ($su_3 \rightarrow ad$)

Under adiabatic conditions the compression work can be calculated from the first law of thermodynamics for closed systems:

$$\dot{W}_{comp} = \dot{m}_{ad}(u_{ad} - u_{su3}) \tag{19}$$

The parameter f_p is a key parameter in this process because how said before is equal at the ratio of the specific volume before and after the compression.

$$f_p = \frac{v_{ad}}{v_{su3}} \tag{20}$$

This is one of the parameters that have to be calibrated.

VI. Isochoric adiabatic expansion/compression (ad → ex)

This transformation can be a compression or an expansion and this can be fixed by the f_p parameter. The higher is f_p the higher is the specific volume v_{ad} and the lower the pressure p_{ad}, if the pressure at the end of the isentropic compression is lower the outlet pressure plus the discharge pressure drop this transformation it will be a compression. Viceversa if p_{ad} is higher of the pressure p_{ex}.

VII. Internal leakages (ex → L)

The internal leakages are computed as an isentropic adiabatic flow through a nozzle, just like the supply losses. The leakage mass flow rate is given as:

$$\dot{m}_{leak} = A_{leak}\sqrt{\frac{2(p_{ex} - p_L)}{v_{ex}}} \tag{21}$$

$$A_{leak} = A_{leak,nom}\left(\frac{f}{f_{nom}}\right) \tag{22}$$

Where p_L is equal at the inlet pressure (p_{su0}).

The fictitious leakages area is proportional at the ratio between the actual and nominal frequency of the motor [3] to take into account the performance drop of check valves at high frequency, the $A_{leak,\,nom}$ parameter has to be calibrated like the suction cross area.

VIII. Isobaric exhaust heat exchange (ex → ex_1)

This heat exchange is computed like the previous but in this case the flux of the heat

is from the fluid to the shell as in figure 26.

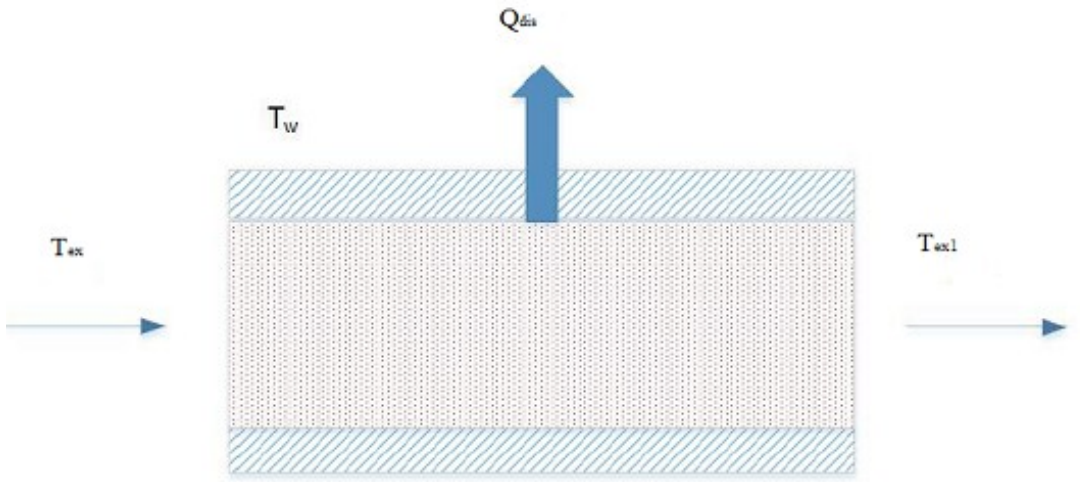

Figure 26: *Isobaric exhaust heat exchange.*

The equations used in this process are:

$$Q_{ex} = \dot{m}_{ex}(h_{ex1} - h_{ex}) \tag{23}$$

$$Q_{ex} = (1 - e^{\frac{-AU_{ex}}{\dot{C}_{ex}}})\dot{C}_{ex}(T_w - T_{ex}) \tag{24}$$

$$AU_{ex} = AU_{ex,nom}(\frac{\dot{m}_{inl}}{\dot{m}_{nom}})^{0.8} \tag{25}$$

The nominal heat transfer coefficient ($AU_{ex,nom}$) has to be calibrated.

IX. Adiabatic exhaust pressure drop ($ex_1 \rightarrow ex_2$)

The exhaust pressure drop is modelled like the supply pressure drop and the characteristic equation is:

$$\Delta p_{ex} = \frac{1}{2}\frac{\dot{m}_{ex2}^2 \cdot v_{ex1}}{A_{ex}^2} \tag{26}$$

The exhaust cross area (A_{ex}) has to be calibrated.

X. Adiabatic isentropic expansion of the trapped mass flow ($ex_1 \rightarrow 0$)

Due to return stroke of the piston the trapped mass flow undergoes an expansion.

The work that comes from this transformation is neglected to be more conservative, but also because its quantity is very low.

The trapped mass flow rate is calculate using the geometrical parameters:

$$\dot{m}_{trap} = \frac{f_a \cdot V_s \cdot N}{60 \cdot v_0} \tag{27}$$

During this transformation there is no entropy variations, from the first law of the thermodynamic for closed systems:

$$\dot{W}_{\exp} = \dot{m}_{trap}(u_0 - u_{ex1}) \tag{28}$$

As explained in the paragraph 3.2 the parameter f_E is a key parameter in this transformation and is one of the parameters that have to be calibrated.

XI. isochoric adiabatic expansion/compression (0 → 1)

This transformation can be a compression or an expansion and this can be fixed with the f_E parameter. The higher is f_E the higher is the specific volume v_o and the lower the pressure p_0, if the pressure at the end of the isentropic expansion is lower the inlet pressure minus the supply pressure drop this transformation it will be a compression. Viceversa if p_0 is higher of the pressure p_1.

Required Work

The work required at the pump shaft is computed as a sum of more terms, the hydraulic work transferred to the fluid is:

$$\dot{W}_{hyd} = \dot{W}_{comp} + \dot{W}_{dis} - \dot{W}_{adm} \tag{29}$$

Where $\dot{W}_{comp}$ is the comprehension work defined before in the transformation $su_3 \rightarrow ad$, $\dot{W}_{dis}$ and $\dot{W}_{suc}$ are the discharge and admission work respectively. The discharge work refers to the power consumed in order to drive the fluid out of the chamber, it correspond to the process $ex \rightarrow ex_1$ in figure 20. and is work provided under constant pressure. While the admission work refers to the power delivered during the suction process of the fluid into the chamber and correspond to the process $su_2 \rightarrow su_3$ in figure 20. The method to count the discharge and the admission work

follow the concept in [8] but the equations are adapted at the pump cycle and the different geometrical parameters. These two terms are computed as:

$$\dot{W}_{dis} = \frac{p_{ex1} \cdot V_s (f_p - C) N}{60} \tag{30}$$

$$\dot{W}_{adm} = \frac{p_{su3} \cdot V_s (1 - f_a) N}{60} \tag{31}$$

Where $V_s(f_p\text{-}C)$ is the volume shift of the chamber during the whole discharge process (from the moment the outlet valves open until they close) and $V_s(1\text{-}f_a)$ is the volume shift of the chamber during the whole suction process (from the moment the inlet valves open until they close).

To obtain the work at the pump shaft is necessary add the mechanical losses ($\dot{W}_{loss}$) caused by the internal frictions:

$$\dot{W}_{sh} = \dot{W}_{hyd} + \dot{W}_{loss} \tag{32}$$

The mechanical losses are calculated using the method proposed by Declaye in [3]:

$$\dot{W}_{loss} = T_{mech} \cdot f \tag{33}$$

Where T_{mech}[Nm] is a constant parameter that has to be calibrated.

Mechanical losses are due to friction and losses in the bearings, these are dissipated as heat into the environment . In the present modelling, all these losses are lumped into one unique mechanical loss torque T_{mech}.

Finally using the motor electric efficiency extrapolate from the manufacturer data (chapter 2) and the frequency driver efficiency, it is possible obtain the electric power:

$$\dot{W}_{el} = \dot{W}_{sh} \cdot \eta_{mot} \cdot \eta_{fd} \tag{34}$$

$$\eta_{fd} = 0.92 \tag{35}$$

The frequency driver efficiency is a constant precautionary value.

Overall heat balance

The thermal equilibrium of the pump is in steady-state conditions and is possible calculate the wall temperature T_w from this, the heat balance is:

$$Q_{amb}+Q_{ex}+Q_{su}-\dot{W}_{loss}=0 \tag{36}$$

Where Q_{amb} is heat transfer from the pump shell to the ambient and is calculated as:

$$Q_{amb}=AU_{amb}(T_w-T_{amb}) \tag{37}$$

Where T_{amb} is the ambient temperature and AU_{amb} (W/K) is the heat transfer coefficient that must be identified through the model calibration procedure.

Pump efficiency

Four efficiencies are defined to measure the performance of the pump, these are the isentropic efficiency:

$$\eta_{is}=\frac{h_{is}-h_{su0}}{h_{ex2}-h_{su0}} \tag{38}$$

the filling factor (or volumetric efficiency):

$$\eta_{vol}=\frac{\dot{m}_{inl}}{\frac{N\cdot V_s\cdot(1-C)}{60\cdot v_0}} \tag{39}$$

that represents the volume flow rate that passes through the pump related to the theoretical volume flow rate that the pump can manage according to its swept volume, the filling factor expresses a relative measure of the internal leakages and the grade of expansion of the trapped mass.

The mechanical efficiency:

$$\eta_m=\frac{\dot{W}_{hyd}}{\dot{W}_{sh}} \tag{40}$$

and the global efficiency that measures the quality of the global process from the electric grid to the working fluid:

$$\eta_{gl}=\frac{V_{flow,inl}(p_{out}-p_{inl})}{\dot{W}_{el}} \tag{41}$$

3.6 Calibration of the model

The calibration of the model consists in fit the experimental data in several working condition with the model results. The fitted experimental data are the mass flow rate and the outlet temperature of the working fluid, the shaft power is given from the manufacturer by the equation 43. A function to calculate the error between calculated value and experimental data is implemented and has to be minimized.

The error equation is:

$$error = \sqrt{\sum_{1}^{n} \left(\frac{\dot{m}_{cal} - \dot{m}_{meas}}{\dot{m}_{meas}}\right)^2} + \sqrt{\sum_{1}^{n} \left(\frac{\dot{W}_{sh,cal} - \dot{W}_{sh,man}}{\dot{W}_{sh,man}}\right)^2} + \sqrt{\sum_{1}^{n} \left(\frac{T_{out,cal} - T_{out,meas}}{T_{out,meas}}\right)^2} \quad (42)$$

$$\dot{W}_{sh.man} = \frac{15 \cdot N}{84428} + \frac{V_{flow} \cdot \Delta p}{511} \quad (43)$$

In the equation 43. N[RPM], V_{flow}[l/min] and Δp [bar] are experimental data in each operating point.

To minimize this equation eleven parameters have to be calibrated, these parameters are:

- AU_{amb} (W/K)
- $AU_{ex.nom}$ (W/K)
- $AU_{su,nom}$ (W/K)
- A_{ex} (m^2)
- A_{su} (m^2)
- $A_{leak,nom}$ (m^2)
- V_h (m^3)
- C
- f_p
- f_E
- T_{mech}

The process flow diagram of the parameters identification (or equivalently of the model calibration) procedure is depicted in figure 27.

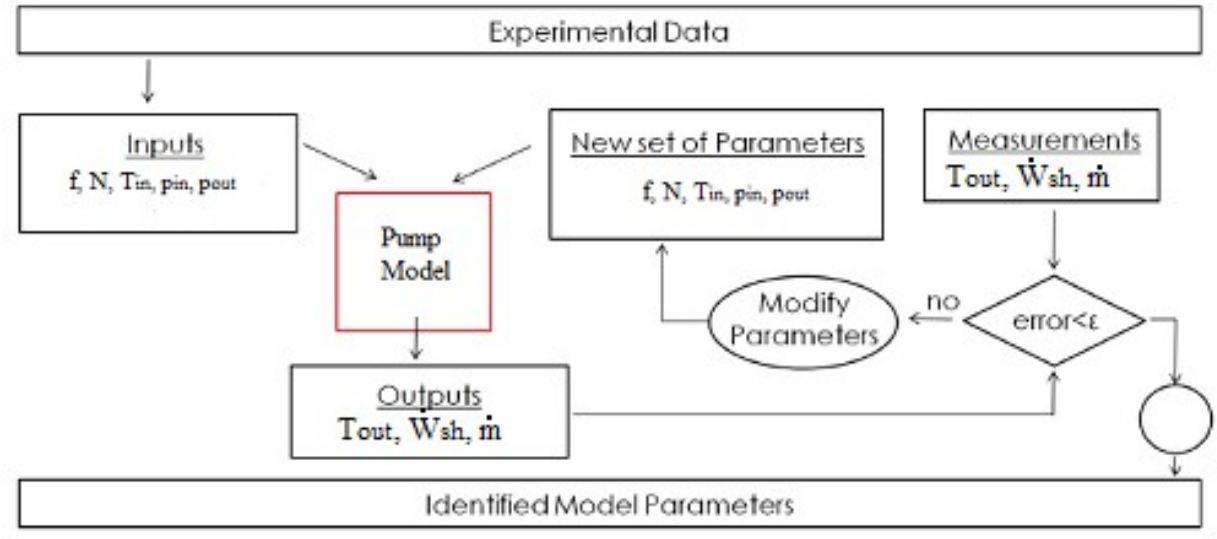

Figure 27: *Process flow chart of the Identification procedure of the model parameters*

Also the inputs f, N, T_{in}, p_{in}, p_{out} are experimental data from the unit.

Results of the calibration:

The calibration is done minimizing the error for 20 different operational point using the Variable metric method available on EES, the results are:

$\mathbf{AU_{amb}}$	**(W/K)**	1
$\mathbf{AU_{ex,nom}}$	**(W/K)**	50
$\mathbf{AU_{su,nom}}$	**(W/K)**	60
$\mathbf{A_{ex}}$	**(m^2)**	0,00007
$\mathbf{A_{su}}$	**(m^2)**	0,00005
$\mathbf{A_{leak,nom}}$	**(m^2)**	0,0000003
C	**(-)**	0,1
$\mathbf{V_h}$	**(m^3)**	0,00002
$\mathbf{f_p}$	**(-)**	0,9945
$\mathbf{f_E}$	**(-)**	1,01
$\mathbf{T_{mech}}$	**(Nm)**	4,28

Table 1: *Results of the calibration.*

It is possible see the relative error in each point in the following graphics, the relative error is always below the 10%.

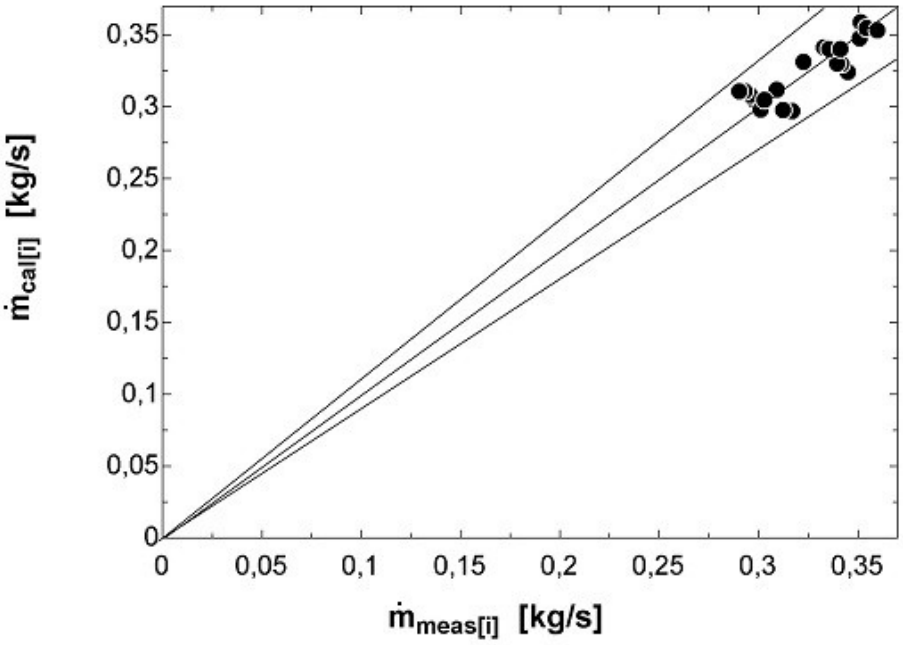

Figure 28: *Calculated mass flow respect the measured mass flow.*

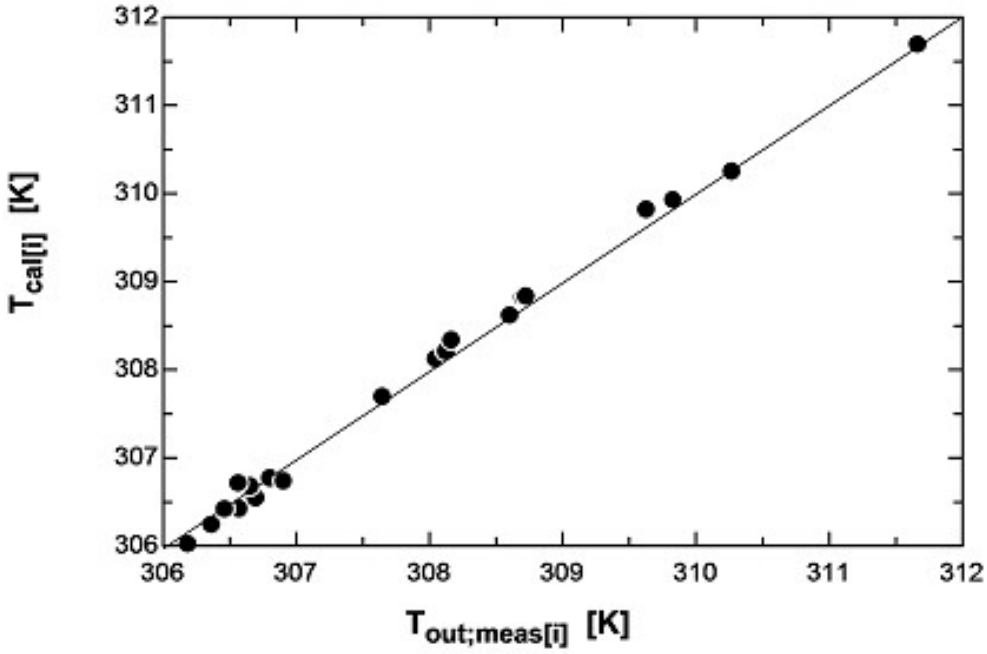

Figure 29: *Calculated outlet temperature respect the measured outlet temperature.*

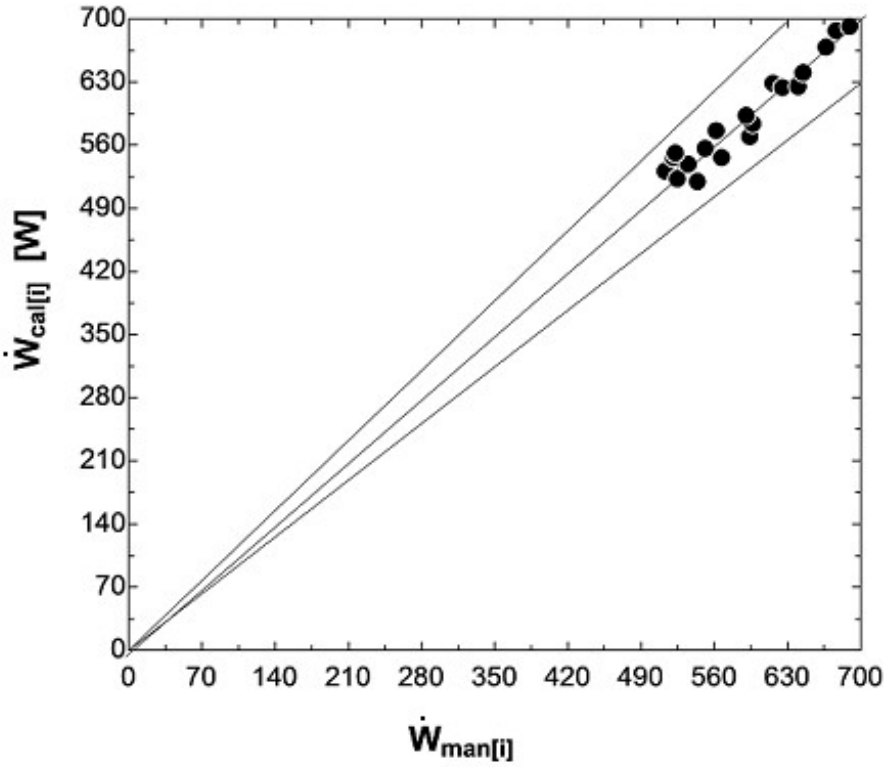

Figure 30: *Calculated shaft power respect the manufacturer shaft power.*

Chapter 4

Analysis of the main parameters

After the calibration and the determination of the eleven independent parameters it is made the analysis of the behaviour of the pump. The analysis uses the same model of the calibration but with the values of the independent parameters (x_i) fixed, then it is, as a matter of fact, an off-design analysis. Then are chosen arbitrary parameters as inputs in order to have as outputs the performance parameters of the pump.

4.1 Characteristics maps

Firstly are compare the model maps with the manufacturer maps, in figure 31. the mass flow rate is compared:

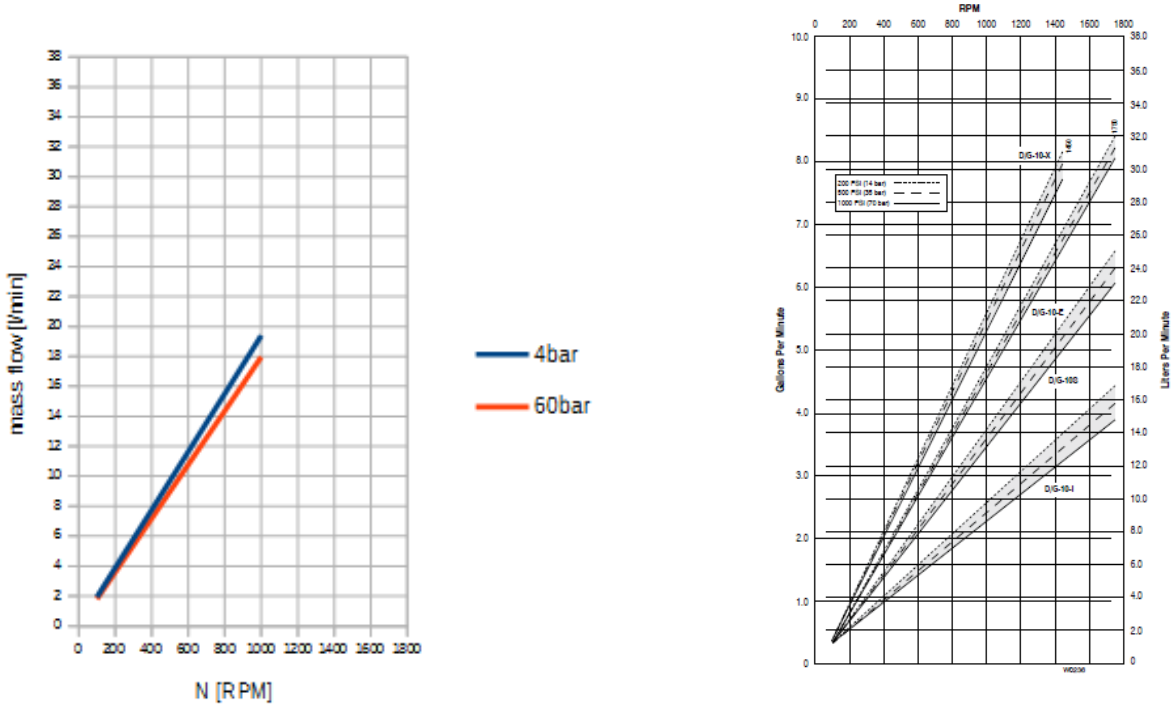

Figure 31: *Outlet mass flow Vs rotational speed maps by the model and manufacturer.*

It is possible see a good accordance between the manufacturer and model map. Considering the curve of the pump D/G-10-X, that is the used model, the values of the mass flow for different rotational speed are very close to the values obtained by the EES model and it is to consider that are not included the different operational conditions and working fluid.

The computed map is done for two different outlet pressure (Δp = 4- 60 bar) and in accordance with the manufacturer curve the higher the Δp and the lower the slope of the curve.

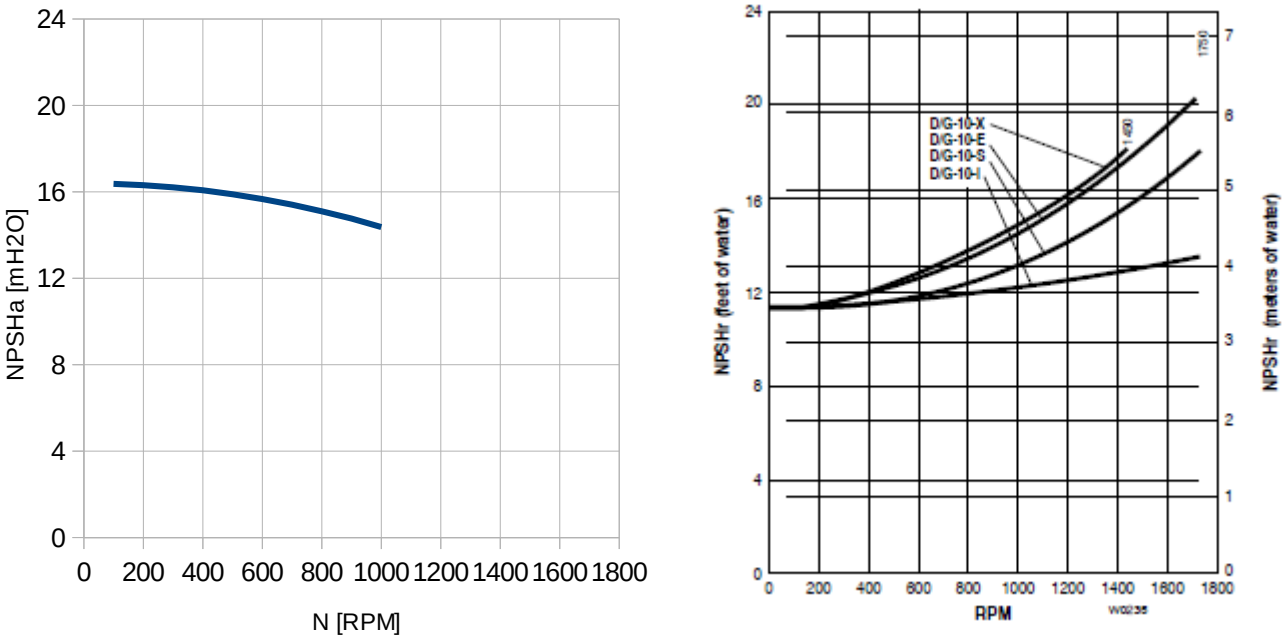

Figure 32: *Variation of the NPSH with the speed rotation by the model and manufacturer.*

The Δ_{NPSH} is calculate with the characteristics of the experimental unit that it will be explained in the next chapter. Here (figure 32.) it is possible see the accordance between the two graphics: the manufacturer propose an exponential grow of the NPSH required and in the model the NPSH available go down with a similar way but opposite. Considering that in the computed curve the NPSHr is kept constant, this means that the NPSHa is decreasing with the speed rotation and because of this the

manufacturer proposes a growing NPSHr curve.

The next comparison is done with the experimental result given by Declaye in [3]. The figure 33. shows how change the global efficiency with the pressure difference and considering the multi-diaphragm pump the graphics are very similar, for the same pressure ratio the value of the global efficiency is quite similar.

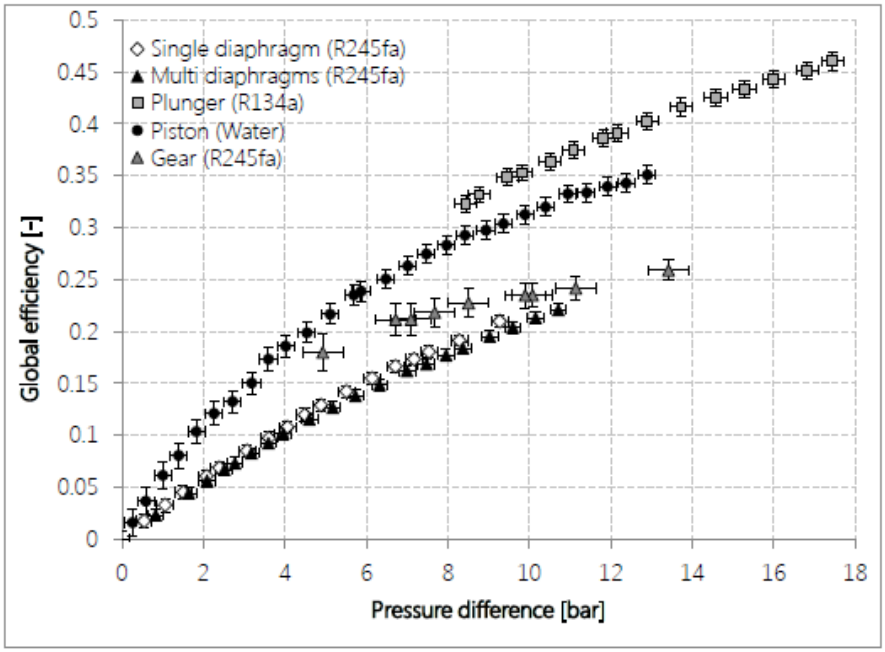

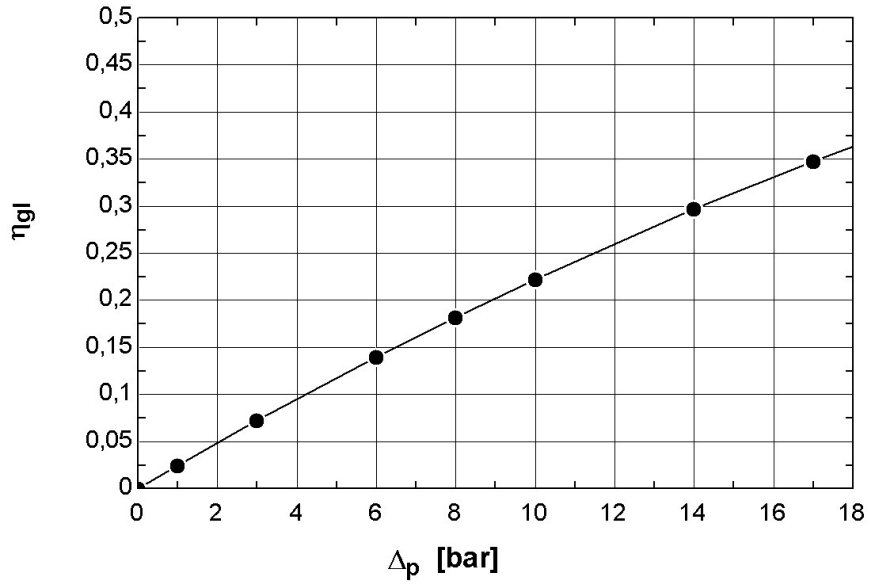

Figure 33: *Global efficiency Vs pressure difference by the model and [3].*

It is to consider that the two graphics are made in totally different conditions, considering the instrumentation of the experimental units.

Like the previous figure also the figure 34. makes a comparison between the current work and the research by Declaye in [3], in this case it is taken into account the volumetric efficiency.

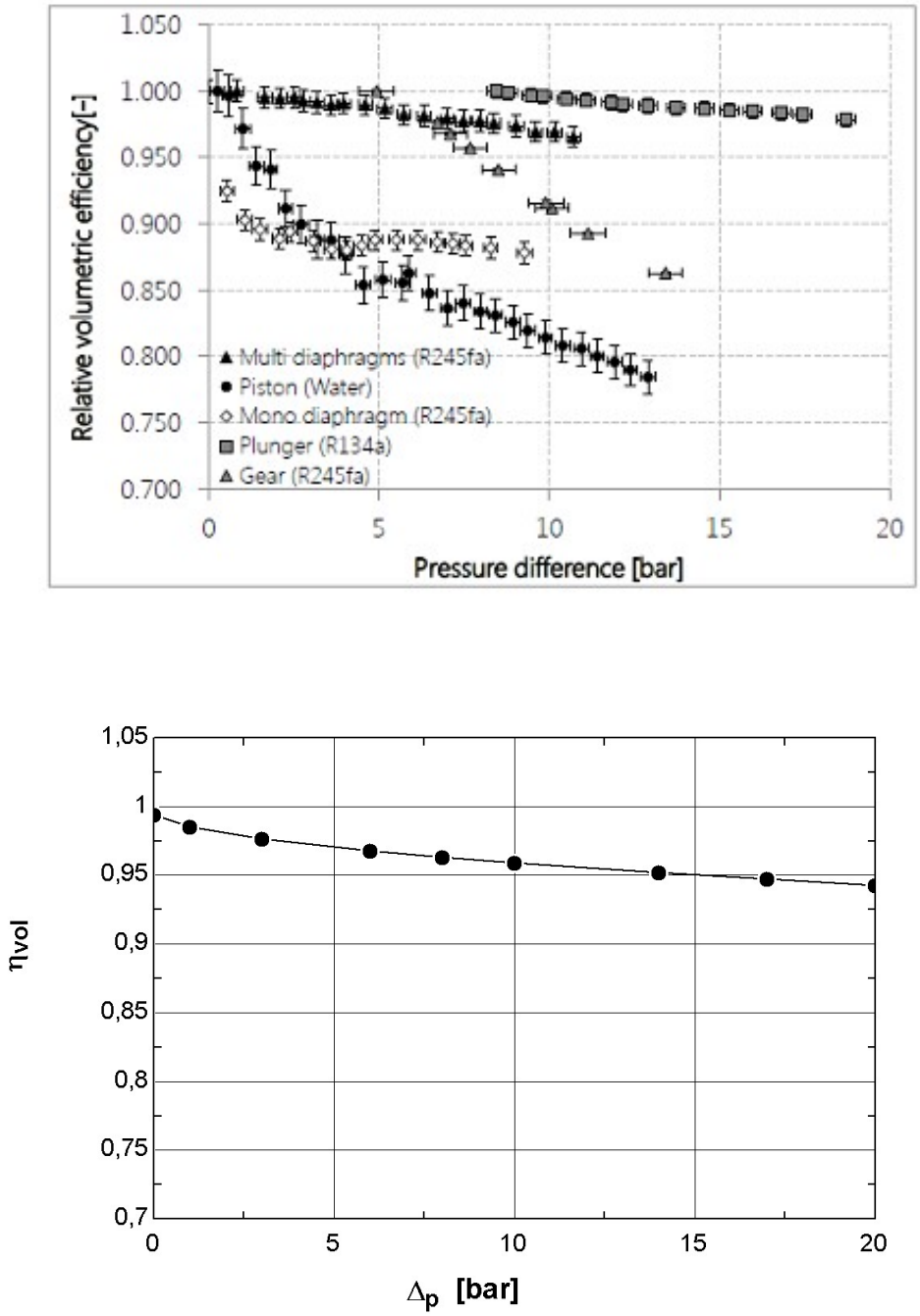

Figure 34: *Volumetric efficiency Vs pressure difference by the model and [3].*

The model has a good fit of the experimental result in [3]. The decrease of the volumetric efficiency with the pressure difference is due to the growing of the leakages and also because the wall temperature increases and as a consequence the specific volume during the suction phase grow.

It is also interesting analyse these two parameters for different value of the speed rotation.

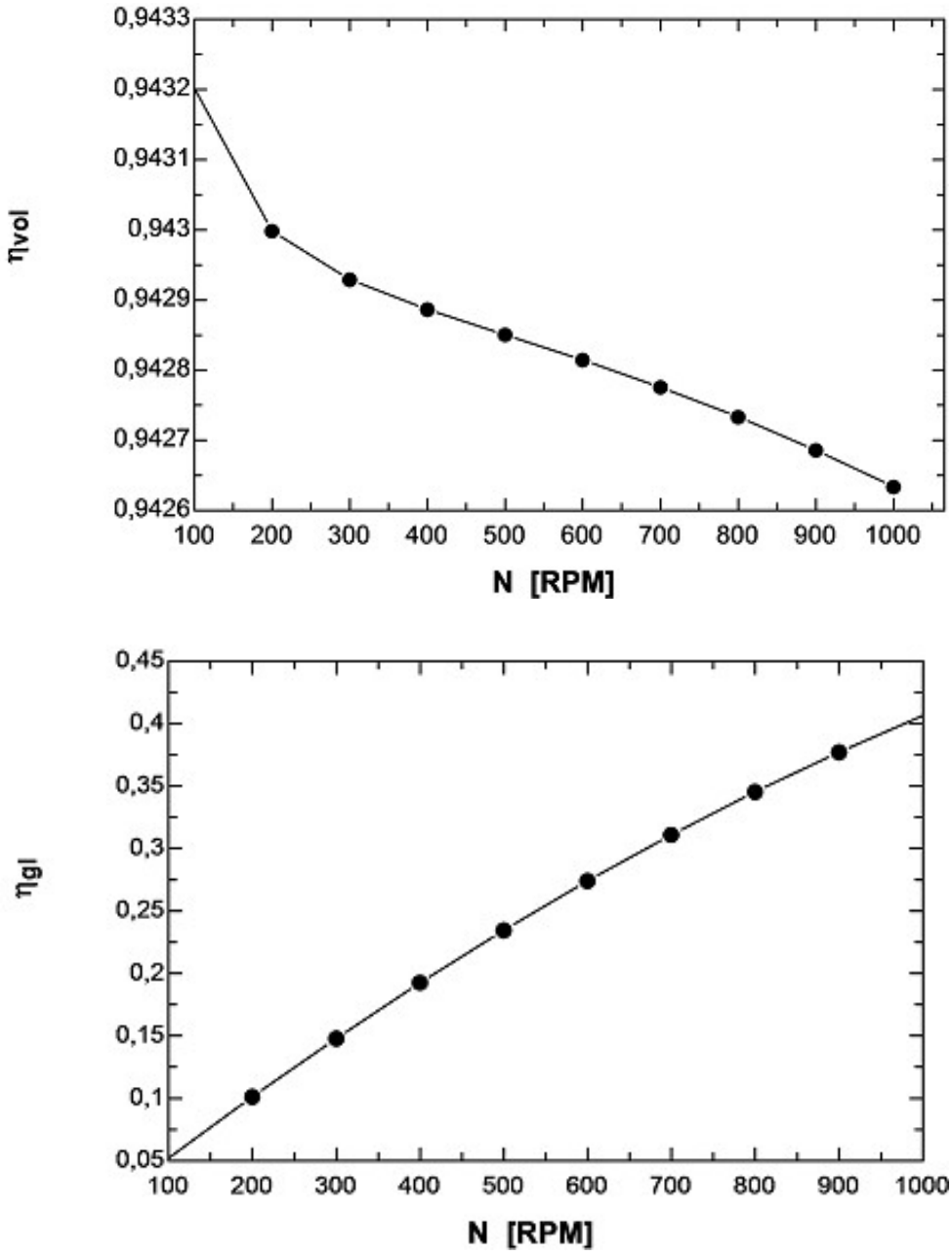

Figure 35: *Global and volumetric efficiency respect the speed rotation.*

The global efficiency increases with the speed rotation even though the mechanical losses increase, this because the mass flow grows with N and as a consequence the hydraulic work given to the fluid, that is the numerator of the global efficiency, grows (eq.41). On the other side the volumetric efficiency decreases because the cross area of the leakages and the mechanical losses increase with the frequency of rotation (eq.22-33) and as a consequence of the mechanical losses the specific volume during the suction phase increases because of an increase of the wall temperature.

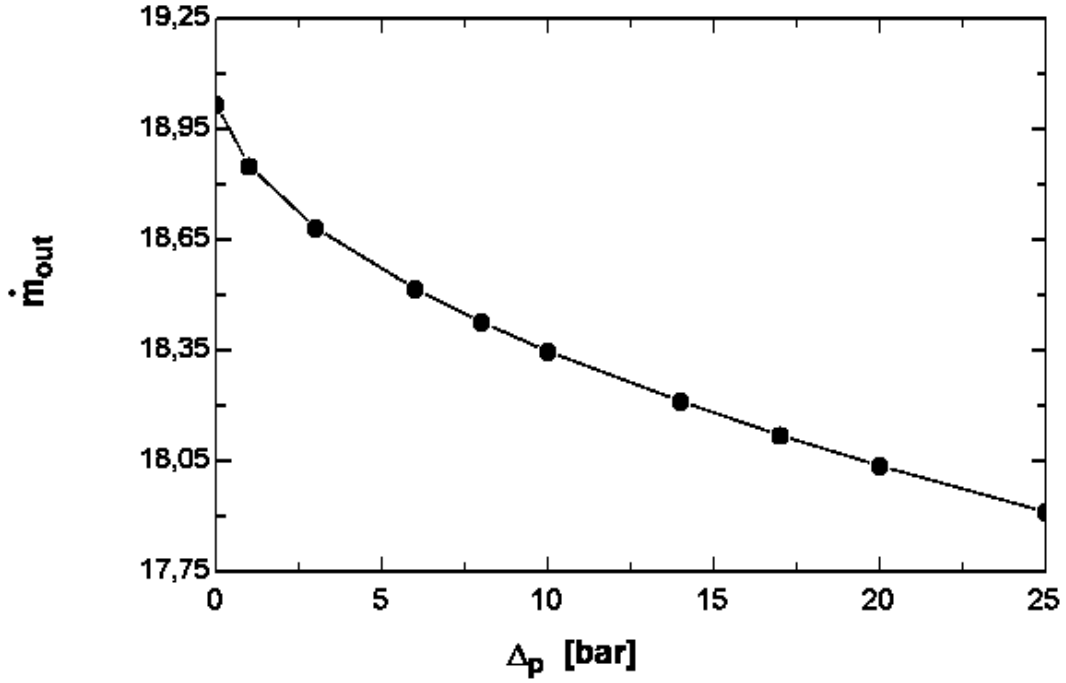

Figure 36: *Outlet mass flow in function of the pressure difference.*

In the figure 36. it is possible see a concordance between the behaviour of outlet mass flow and the volumetric efficiency (figure 34.), the decrease of the outlet mass flow follows the same reasons of the decrease of the volumetric efficiency.

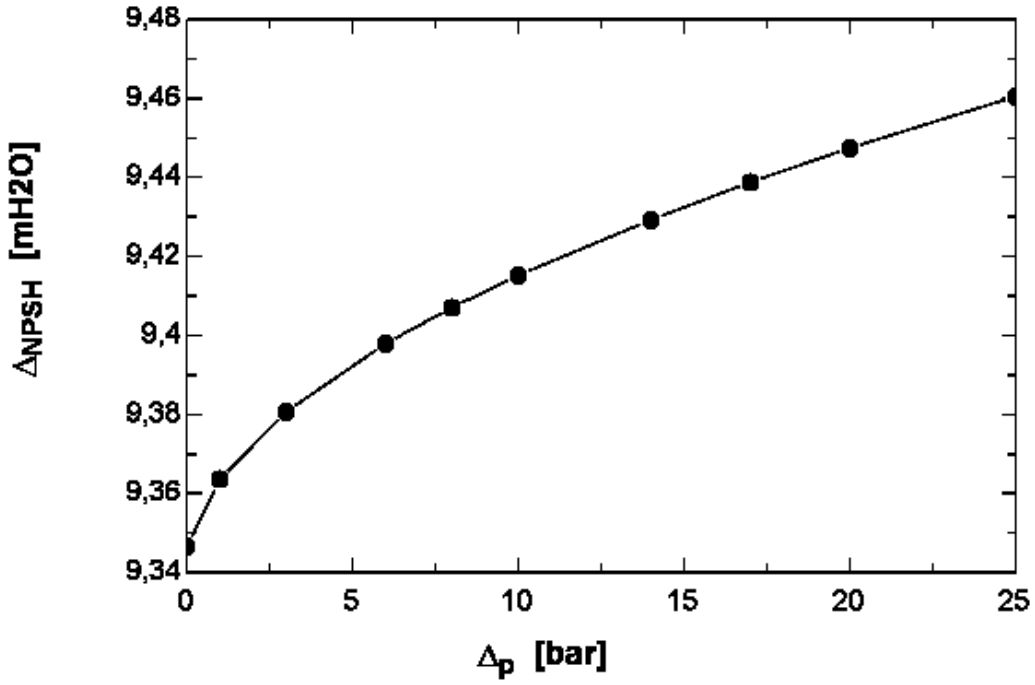

Figure 37: *Variation of the Net Position Suction Head with the pressure difference.*

Figure 37. shows how the Net Position Suction Head available is influenced by the outlet pressure. The NPSH available increases with the pressure difference because as figure 36. shows the mass flow decreases and this produce a decrease of the acceleration head losses (the H_a term explained in the next chapter) at the suction port.

The last sensitivity analysis regards the variation of the electric power with the pressure difference and the speed rotation (figure 38.).

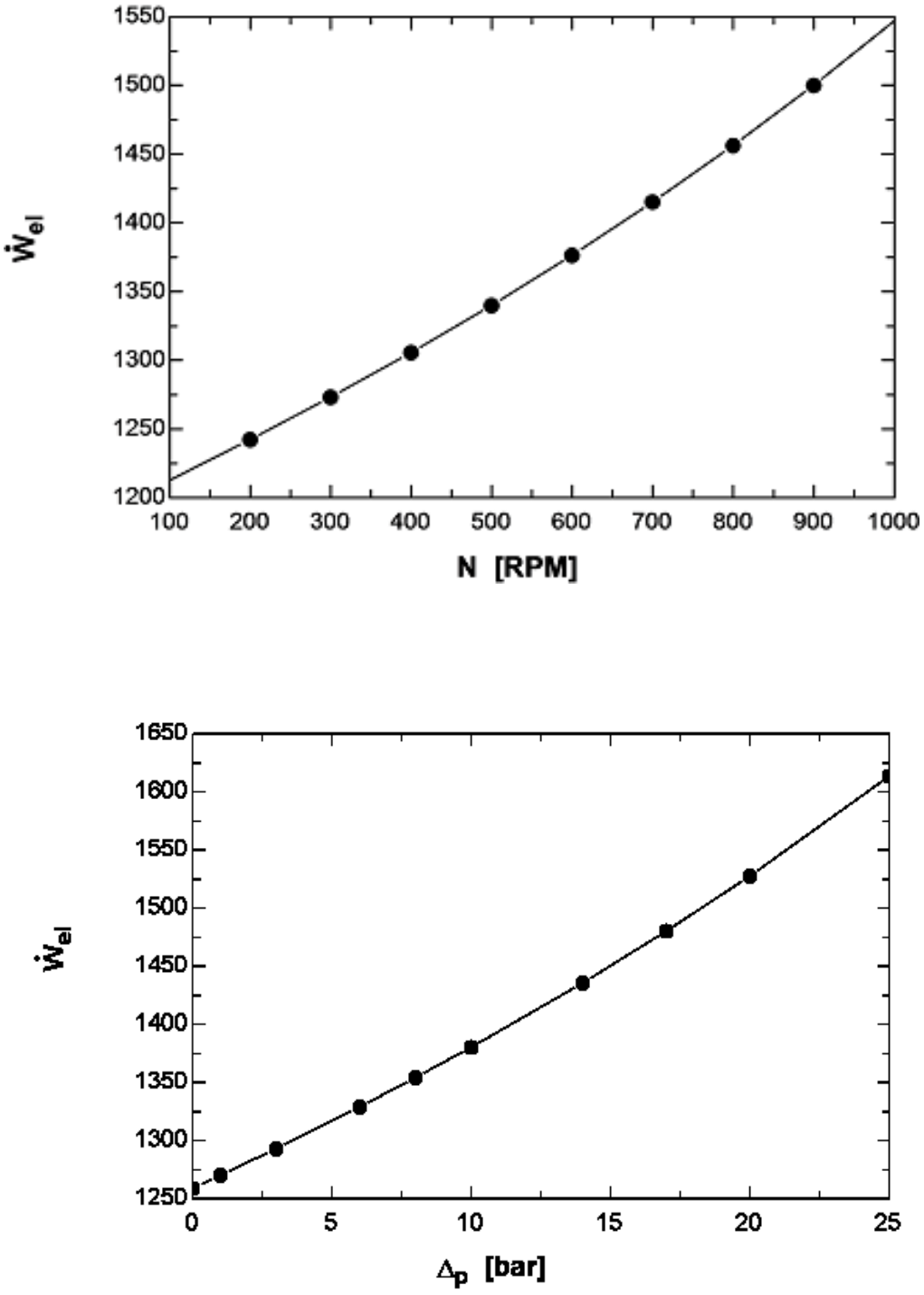

Figure 38: *Electric power in function of the pressure difference and the speed rotation.*

It is interesting see that the electric power for low value of Δp and N is still around 1kW, that because even though the shaft power is very low the electric motor works in a strong inefficiency zone and the global efficiency is very low (figure 32-34).

Chapter 5

Analysis of the cavitation

In this chapter it is presented the analysis of the model in cavitation condition in order to find and predict this issue. As described in the introduction, cavitation condition implies not only inefficiency for the pump but for the whole ORC unit. It is important to be able to predict in different operational condition when the cavitation happens and avoid it without losing in terms of efficiency of the plant (figure 3.).
In this chapter is not considered as inlet pressure the pressure at the suction port of the pump, as the previous analysis, but the pressure at the feed tank outlet (positioned just before the pump) to have a good match between the experimental work and the semi-empirical model.

5.1 The cavitation in the experimental unit

From tests on the experimental unit it was found that the pump goes to cavitate in different operational conditions. It is reported part of the work in [7] to present the problem and how it has been solved.
To ensure stable operation of a pump, the **available** Net Positive Suction Head (NPSHa) at the pump inlet should exceed the respective **required** Net Positive Suction Head (NPSHr), given by the operation curves provided by the manufacturer, by at least 100mbar or an equivalent of 1 mH2O. The NPSHa (mH20) is calculated by the following equation:

$$NPSHa = p_{atm} + H_z - H_f - H_a - pvp \tag{44}$$

Where:

p_{atm} = Atmospheric pressure

H_z = Vertical distance from surface liquid to pump center line (if liquid is below

pump center line, the H_z is negative)

H_f = Friction losses in suction piping

H_a = Acceleration head at pump suction

pvp = Absolute vapour pressure of liquid at pumping temperature

The acceleration head factor (H_a) is calculated by equation 45.

$$H_a = \frac{C \cdot L \cdot Vel \cdot N}{K \cdot G} \quad (45)$$

Where:

C = Constant determined by type of pump (Wanner Engineering, Hydra Cell D/G10)

L = actual length of suction line

Vel = Velocity of liquid in suction line

N = RPM of crank shaft

G= Gravitational constant

K = Constant to compensate for compressibility of the fluid

In the experimental work in [7] it is used in the equation 44. the pressure at the outlet of the tank and the term H_f is estimated in order to take into account also the kinetic factor. For the operating conditions at the design point of the experimental unit the NPSHr is 500mbar, H_z=0,3m, H_a≈200mbar, and H_f=200mbar.

The follow description of the unit behaviour in cavitation conditions and the next solution at the problem is taken from [7].

The main parameters of the ORC feed pump under operation with cavitation effect are depicted in Figure 39. In fact, the ORC pump was tested while just circulating the refrigerant around the ORC circuit via the scroll by-pass section and thus practically no pressure raise is implemented by the pump. Analyzing the pump operation at the first oscillation cycle (cold start), it is observed that initially the pressure at the pump inlet/outlet remains constant with time, indicating a constant mass flow rate, and that the NPSHa - NPSHr difference is maintained well above the threshold of 100mbar (1 mH2O). As the whole system is ramping up, the temperature at the condenser outlet

raises due to the increase of the evaporator outlet temperature. Consequently, the temperature at the pump inlet raises but with a significant time lag caused by the thermal inertia of the feed tank, which stands between the condenser outlet and the pump inlet. With raising temperature at the pump inlet, the absolute pressure of the refrigerant (factor pvp of eq.44) raises and as a result the NSPHa drops. When the difference NPSHa – NPSHr reaches a critical value of around 100mbar (1 mH2O), the cavitation effect is initiated and the circulating mass flow rate drops significantly. Simultaneously, the pressure of the circuit (controlled by the condensation temperature which drops due to the reducing refrigerant mass flow rate) also drops and the unit's operation practically collapses. To make things worse, even though at this point the refrigerant temperature at the condenser outlet drops dramatically, since there is practically a zero mass flow rate, the feed tank needs time to cool down and keeps feeding the pump at relatively high temperature (and thus high Pvp); at this point the NPSH difference is strongly negative. Eventually the feed tank cools down, lowering the pumping temperature and thus raising the NPSH difference. Gradually the cavitation effect fades, the mass flow rate raises, and a new cycle starts over.

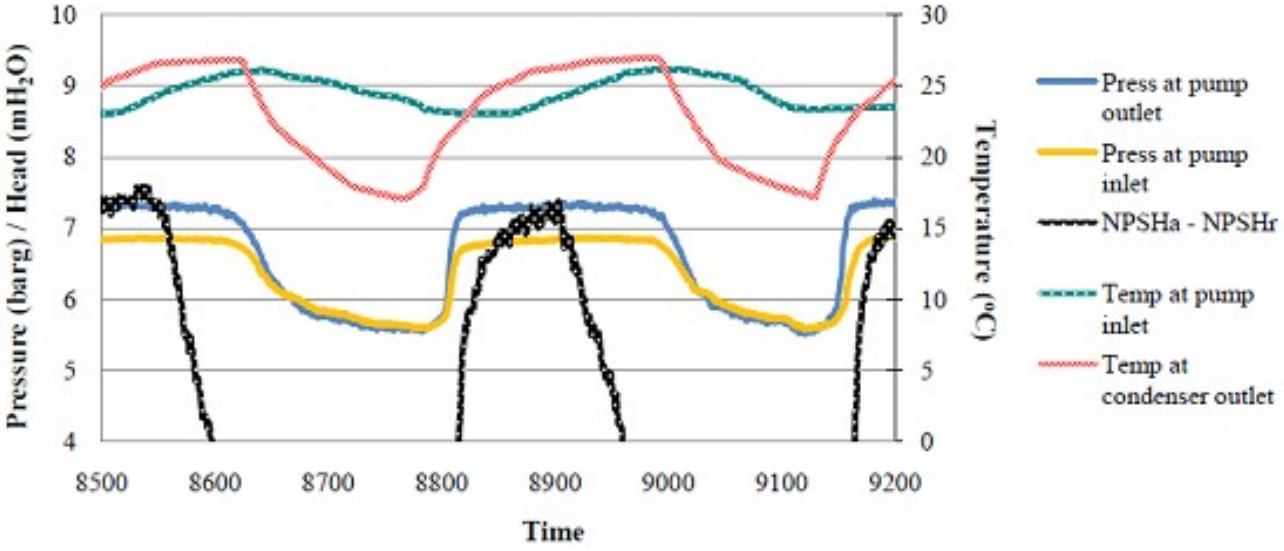

Figure 39: *Cavitation effect on ORC pump operation. From [7]*

In order to solve this problem a water cooled heat exchanger was installed in the suction line of the ORC pump, downstream of the liquid receiver, so that the pumping temperature and thus the absolute pressure of the refrigerant (factor pvp of eq.44) are maintained at lower values, ensuring stable pump operation. The main parameters of the ORC pump under operation with the additional sub-cooling heat exchanger are depicted in Figure 40. The measurements have been obtained at similar operation conditions with Figure 38., allowing their direct comparison. The sub-cooling heat exchanger causes an average 2K temperature drop at the suctioned refrigerant which has proved to be sufficient for the stable operation of the unit. As it can be seen in the diagram, the NSPHa is constantly kept above 17 mH2O with a required NPSH of 5 mH20. Its main fluctuations are caused by the suction pressure, which in turn depends on the cooling water mass flow at the condenser (or equivalently on the condenser outlet temperature) and naturally by the temperature at the pump inlet which affects the factor pvp as already discussed. Accordingly, between t=300 and t=690 the NPSHa is slightly dropping even though the suction pressure is slightly raising, due to the greater influence of the raising temperature at the pump inlet (factor Pvp). The evident drops of NPSHa at t=700, t=840 and 1040 are caused by marginal steps of increasing cooling water mass flow rate at the condenser which directly influence the pressure at the pump inlet and thus the NPSHa. At the respective intervals the observed NPSHa raise is caused by the slightly decreasing temperature at the pump inlet. It is finally noted that the stable operation of the feed pump can be confirmed by the observation of the almost constant delivered Head of the pump over time (Pout-Pin).

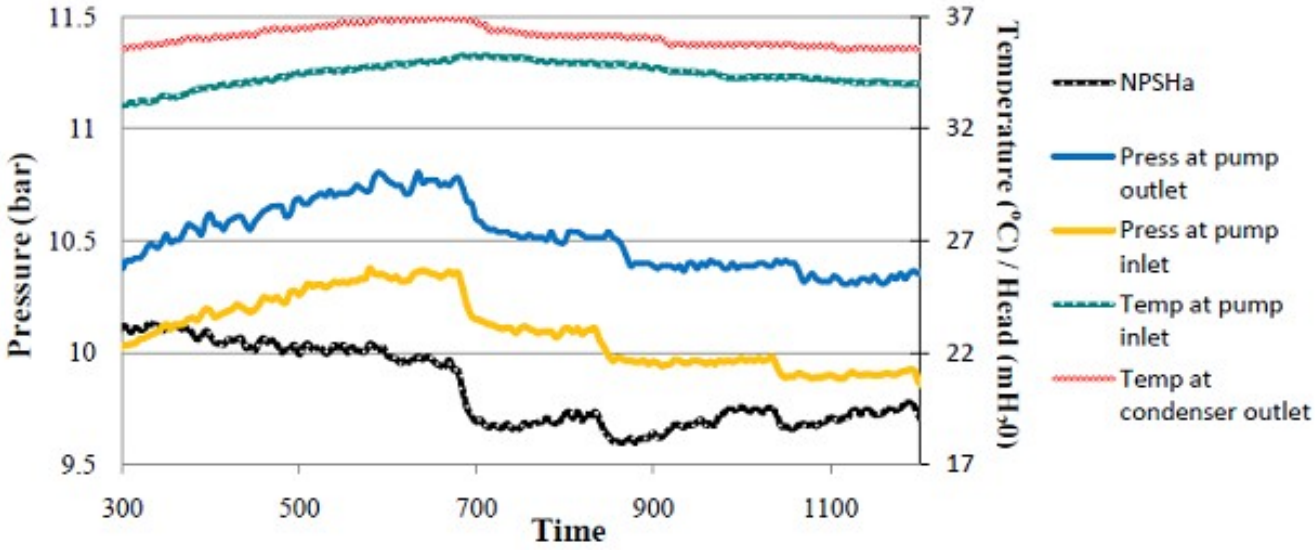

Figure 40: *ORC pump operation with the addition of a sub-cooling heat exchanger. From [7]*

5.2 Cavitation prediction with the semi-empirical model

To calculate the available NPSH with the model it is used the follow equation:

$$NPSHa = p_{tank} + H_z - H_f - H_a - pvp \quad (46)$$

Where p_{tank} is the outlet pressure of the tank and the others terms are the same in the equation 44. The inlet pressure of the pump is equal at the outlet pressure of the tank plus the H_z term and minus the H_f term, because as said before these terms take into account the variation of the kinetic energy.

Due to the equation of the acceleration head (H_a) that changes its value in function of the velocity of the liquid in the suction line and the speed rotation of the pump, it is implemented in the model an equation that takes into account these variations. Considering that the estimated value of H_a in nominal operating conditions of the plant is 200mbar [7], in different work conditions is determined by the equation 47.:

$$H_a = \frac{200\,mbar}{V_{flow,inl,DP} \cdot N_{DP}} (V_{flow,inl} \cdot N) \quad (47)$$

Where:

$V_{flow,inl,DP}$ = Inlet volumetric flow rate at the design point of the unit (20 lt/min)

N_{DP} = Pump speed rotation at the design point of the unit (960 RPM)

$V_{flow,inl}$ = Inlet volumetric flow rate

N = Pump speed rotation

The velocity of the fluid in the suction line is replaced by the inlet volumetric flow rate because of the continuity equation of the mass:

$$Vel = \dot{m} \cdot v \cdot A \tag{48}$$

Where Vel is the velocity (m/s), ṁ the mass flow rate (kg/s), v the specific volume (m^3/kg) and A the cross area (m^2). The cross area is the same in the different operating conditions, then velocity variations are due to mass flow rate and the specific volume that together form the volumetric flow rate.

Also the friction losses have a dependence with the velocity of the fluid, in the model this term changes with the square of the volumetric flow rate:

$$H_f = 200\,mbar \left(\frac{V_{flow,inl}}{V_{flow,inl,DP}} \right)^2 \tag{49}$$

Variations of H_f with the Reynolds number are not considered because are also function of the flow regime.

With this procedure are obtained the graphics in the previous chapter (figure 37-32) and the next graphics used to compare the experimental result showed before (figure 39-40.) and the model results in the same operational conditions (figure 41-42.).

The two figures (41-42.) show the same behaviour of the Δ_{NPSH} value of the experimental results (figure 39-40.), this means that the method of calculation implemented in the model is in concordance with the method proposed in [7].

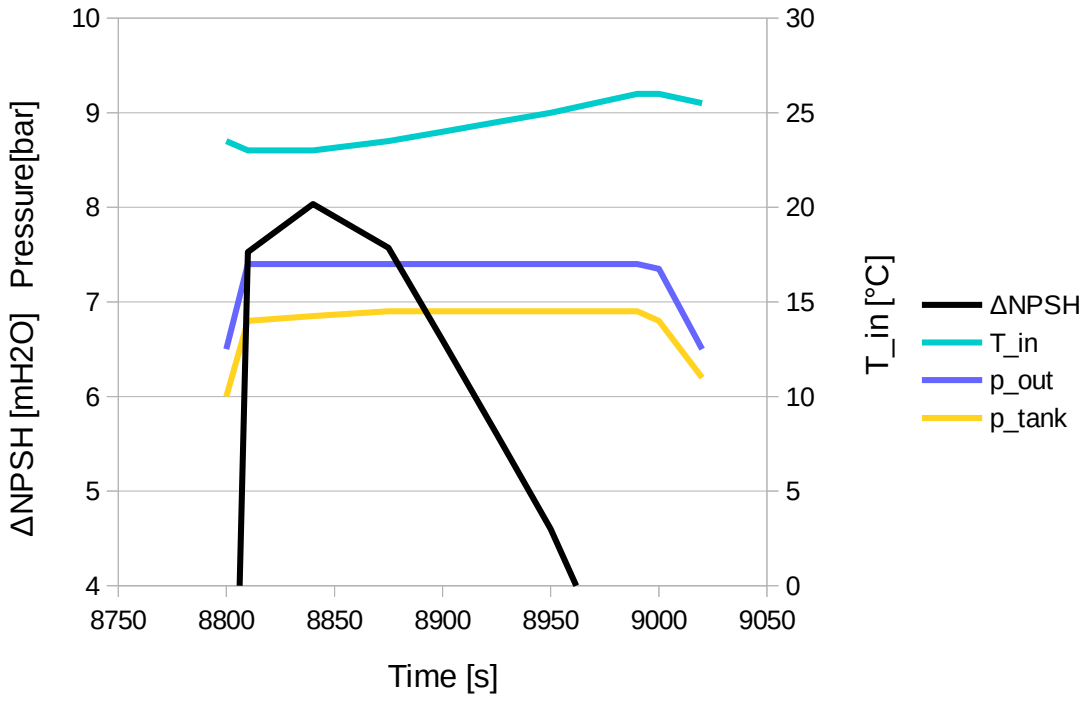

Figure 41: *Model analysis in the same operating condition of figure 39.*

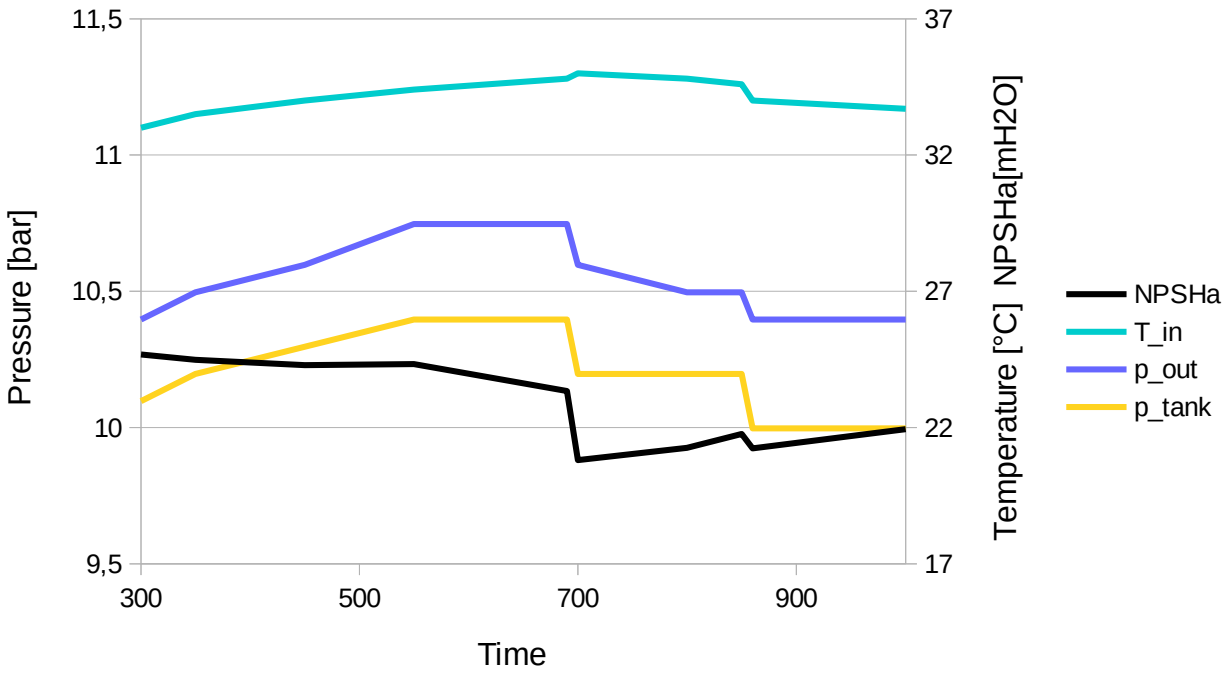

Figure 42: *Model analysis in the same operating condition of figure 40.*

To confirm the match between the semi-empirical model of the pump and the NPSHa

calculation method proposed before need that the model find two-phase fluid condition in the suction phase when the value of the NPSHa calculated is near to zero. With the follow operational conditions:

N = 960 [RPM]

p_{tank} = 10 [bar]

p_{out} = 15 [bar]

the inlet temperature was increased until a value of 37,4°C, where two-phase condition has been found. In these conditions the value of the NPSHa is 2mH2O and the Δ_{NPSH} is -3,124mH2O, also considering what the manufacturer suggest to avoid instabilities (paragraph 5.1) it is possible say that the calibration of the semi-empirical model is in accordance with the terms H_f, H_a, H_z used to calculate the NPSHa.

The work presented by Leontaritis *et al.* [7] talks about a possible cavitation problem for high speed rotation of the pump, this correlation between speed rotation and Δ_{NPSH} is showed in figure (32) and from this graphic is possible see the strong decrease of the available net position suction head when the rotational speed is high.

To have a better understanding of this phenomenon a last analysis is presented in figure 43.

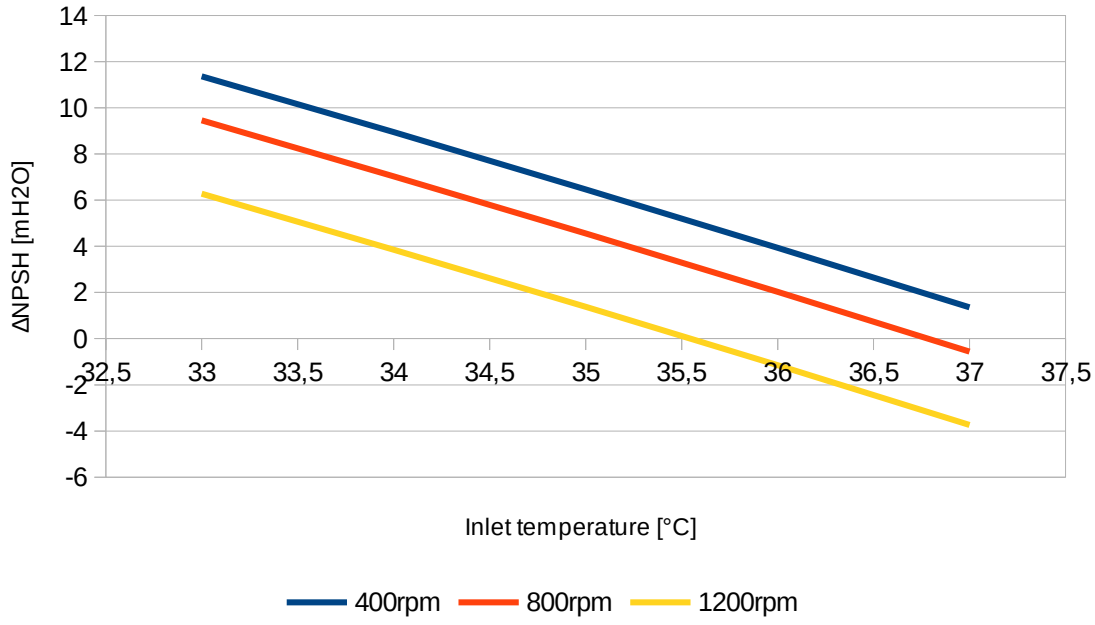

Figure 43: *Cavitation analysis for different speed rotation.*

The analysis is made with pressure and temperature values near the operational conditions of the subcooling case (figure 40-42.):

p_{inl} = 10 [bar]

p_{out} = 15 [bar]

It is possible to see how strong is the influence of the rotational speed, the gap between the Δ_{NPSH} values for 1200rpm and 800rpm is bigger than the gap for 400rpm and 800rpm even though the speed rotation step is the same in the two cases.

The unstable condition (Δ_{NPSH} =1mH2O) is reached for an inlet temperature of 35°C for 1200rpm while for 800rpm and 400rpm the value of Δ_{NPSH} is around 5mH2O and 7mH2O respectively.

Conclusions

In this work a semi-empirical model proposed by V. Lemort *et al.*[4] for a volumetric expander operating with organic fluids is adapted to a R134a displacement pump installed in a ORC system starting from the idea that the expander and the pump operates with the same kind of fluid (organic fluid) and the thermo-fluid-dynamic principles are similar.

The model is first calibrated through a set of experimental data including pressure, temperature and mass flow rate measurements at the inlet and outlet of pump while no experimental data of the power consumption of the pump was available. To overcome this problem manufacturer estimation of the required shaft power in different operating condition is used. The calibration is satisfying due the low relative error for each operating point, less than 10% for the mass flow and the shaft power and less than 0,07% for the outlet temperature.

The calibrated model is than used to evaluate the characteristic curves of the pump and to and to detected potential cavitation conditions. The comparison of the resulting performance and NPSH curves with analogous curves by the manufacturer shows that the model results are in good agreement with information provided by the pump manufacturer. It was found a good match of the model and experimental results also as regards the cavitation prediction. Thus, the model can be used not only to evaluate the pump performance at various load, but also to avoid cavitation in all operating conditions of the plant in which the pump is installed by including a sub-cooling process in the condenser. The sub-cooling produces a decrease in the overall cycle efficiency (Declaye [3]) then the model may be used to calculate the maximum temperature at the pump inlet that are required to avoid cavitation, that corresponds to the minimum sub-cooling of the organic fluid in the condenser.

A critical part of the presented work consists in the shaft power calculation that derives from manufacturer estimation, better results may be obtained in further developments by measuring the shaft power or the electric consumption of the pump in order to improve the model coefficients.

Nomenclature

A	Area, m^2
AU	Heat transfer coefficient, W/K
C	Ratio, -
$\dot{C}$	Heat capacity, W/K
f	Frequency, Hz
f_p	Ratio, -
f_L	Ratio, -
f_a	Ratio, -
g	Gravity acceleration, m^2/s
h	Specific enthalpy, J/kg
H	Altitude difference between the fluid reservoir and the pump, m
H_z	Vertical distance from surface liquid to pump center line, m
H_a	Acceleration head at pump suction, mbar
H_f	Friction losses in suction piping, mbar
$\dot{m}$	Mass flow rate, kg/s
N	Speed rotation, RPM
NPSHa	Available Net Position Suction Head, mH2O
NPSHr	Required Net Position Suction Head, mH2O
p	Pressure, Pa
pvp	Absolute vapour pressure of liquid at pumping temperature, Pa
Q	Heat transfer rate, W
r_w	Back-work ratio, -
r_T	Temperature ratio, -
s	Specific entropy, J/(kg·K)
T	Temperature, K
T_{mech}	Mechanical losses parameter, Nm

u	Specific internal energy, J/kg
v	Specific volume, m^3/kg
V_{flow}	Volumetric flow rate, lt/min
V_H	Swept volume, m^3
V_S	Total volume, m^3
V_0	Dead Volume, m^3
Vel	Velocity, m/s
$\dot{W}$	Power, W

Greek symbols

Δ	Difference, -
η	Efficiency, -
ρ	Density, kg/m^3

Subscripts

ad	Adapted	L	Leakages stream
adm	Admission	leak	Leakage
amb	Ambient	loss	Losses
atm	Atmospheric	m	Mechanical
cal	Calculated	meas	Measured
comp	Compressor	man	Manufacturer
cond	Condensing	mot	Motor
dis	Discharge	nom	Nominal
DP	Design point	out	Outlet
el	Electric	pp	Pump
ev	Evaporating	res	Reservoir
ex	Exhaust	exp	Expansion
sat	Saturation	fd	Frequency driver

sh	Shaft	gl	Global
su	Supply	hyd	Hydraulic
tank	Tank	inl	Inlet
tot	Total	is	Isentropic
tur	Turbine		
trap	Trapped		
vol	Volumetric		
w	Wall		

Bibliography

1. Vincent Lemort, Sylvain Quoilin, Cristian Cuevas, Jean Lebrun, *Testing and modelling a scroll expander integrated into an Organic Rankine Cycle,* Applied Thermal Engineering 29 (2009) 3094–3102.
2. Vincent Lemort, Sylvain Quoilin, Jean Lebrun, *Experimental study and modeling of an Organic Rankine Cycle using scroll expander,* Applied Energy 87 (2010) 1260–1268.
3. Sèbatien Declaye, Vincent Lemort, *Improving the performance of μ-ORC systems,* Phd thesis, Université de Liège, Liège, Belgium (2015).
4. Yulia Glavatskaya, Pierre Podevin, Vincent Lemort, Osoko Shonda, Georges Descombes, *Reciprocating Expander for an Exhaust Heat Recovery Rankine Cycle for a Passenger Car Application,* Energies 2012, 5, 1751-1765.
5. Byrne, P., Ghoubali, R., Miriel, J., *Scroll compressor modelling for heatpumps using hydrocarbons as refrigerants*, International Journal of Refrigeration (2013), doi: 10.1016/ j.ijrefrig.2013.06.003.
6. Arnaud Landelle, Nicolas Tauveron, Philippe Haberschill, Rémi Revellin, Stephane Colasson, *Study of reciprocating pump for supercritical ORC at full and part load operation, 3*rd International Seminar on ORC Power Systems, October 12-14, 2015, Brussels, Belgium, Paper ID: *9*, Page 1.
7. Aris-Dimitrios Leontaritis, Platon Pallis, Sotirios Karellas, Aikaterini Papastergiou, Nikolaos Antoniou, Panagiotis Vourliotis, Nikolaos Matthaios Kakalis, and George Dimopoulos, *Experimental study on a low temperature ORC unit for onboard waste heat recovery from marine diesel engines,* 3rd International Seminar on ORC Power Systems, October 12-14, 2015, Brussels, Belgium, Paper ID: *55*, Page 1.
8. EXP-HEAT, National Technical University of Athens, *Energy recovery in new and retrofitted heat pumps using a dedicated expander concept,* Work Package

4. Report on the simulation of the expander prototype, Athens (2015).

9. Frangopoulos Christos, Kalikatzarakis Miltiadis, *Thermo-economic optimization of synthesis, design and operation of a marine organic Rankine cycle system,* journal of engineering for the maritime environment, Athens (2015).
10. Marco Soffiato, Christos A. Frangopoulos, Giovanni Manente, Sergio Rech, Andrea Lazzaretto, *Design optimization of ORC systems for waste heat recovery on board a LNG carrier,* Energy Conversion and Management 92 (2015) 523–534.
11. Andrea Toffolo, Andrea Lazzaretto, Giovanni Manente, Marco Paci, *A multi-criteria approach for the optimal selection of working fluid and design parameters in Organic Rankine Cycle systems, Applied Energy 121 (2014) 219–232.*
12. N. Mazzi, S. Rech, A. Lazzaretto, *Off-design dynamic model of a real Organic Rankine Cycle system fuelled by exhaust gases from industrial processes,* Energy xxx (2015) 1e15.
13. Lin C, *Feasibility of using power steering pumps in small-scale solar thermal electric power systems,* Bachelor Thesis, Massachusetts Institute of Technology. Dept. of Mechanical Engineering, 2008
14. E. Winandy, C. S. O. and J. Lebrunb, *Simplified modelling of an open-type reciprocating compressor*, Int. J. Therm. Sci. 41, Department of Mechanical Engineering, University of Concepción, Casilla 160, Concepción, Chile, 2002.